Journal of *Marine Science and Engineering*

MDPI

Article

Diagenetic Evolution of Syngenetic Volcanogenic Sediment and Their Influence on Sandstone Reservoir: A Case Study in the Southern Huizhou Sag, Pearl River Mouth Basin, Northern South China Sea

Jiahao Chen [1,2], Hongtao Zhu [1,2,*], Guangrong Peng [3], Lin Ding [3], Zhiwei Zeng [4], Wei Wang [1,2], Wenfang Tao [3] and Fengjuan Zhou [3]

[1] Key Laboratory of Tectonics and Petroleum Resources, China University of Geosciences, Ministry of Education, Wuhan 430074, China; chenjhm@cug.edu.cn (J.C.); wang.wei@cug.edu.cn (W.W.)
[2] School of Earth Resources, China University of Geosciences, Wuhan 430074, China
[3] Shenzhen Branch of the China National Offshore Oil Corporation, Shenzhen 518000, China; penggr@cnooc.com.cn (G.P.); dinglin@cnooc.com.cn (L.D.); taowf@cnooc.com.cn (W.T.); zhoufj@cnooc.com.cn (F.Z.)
[4] School of Geophysics and Geomatics, China University of Geosciences, Wuhan 430074, China; zwzeng@cug.edu.cn
* Correspondence: htzhu@cug.edu.cn

Abstract: The Paleogene sandstone reservoir of Huizhou Sag is an important target for deep exploration in the Pearl River Mouth Basin, South China Sea. Because of the intense volcanic activity, it had a significant impact on the development of reservoirs, making it hard to predict. The diagenetic process of volcanogenic sediment and their influence of the reservoir have been studied by petrographic analysis, X-ray diffraction and scanning electron microscopy (SEM). Four types of volcanogenic sediment were identified: volcanic dust (<0.05 mm), volcanic rock fragments, crystal fragments (quartz and feldspar) and vitric fragments. The strong tectonic and volcanic activity of the Wenchang Formation resulted in a high content of volcanic materials, which led to significant reservoir compaction. The main sedimentary facies types are fan delta facies and lacustrine facies; the thick lacustrine mudstone can be used as high-quality source rock. After the source rock of the Wenchang Formation matured and discharged acids, feldspar and rock fragments dissolved to form dissolution pores, which effectively increases the porosity of the reservoir, but the argillaceous matrix and clay minerals produced by the volcanic dust alteration would reduce the permeability of the reservoir. With the weaker tectonic activity of the Enping Formation, the sedimentary facies changed into braided river delta, resulting in the greater componential maturity of the reservoir. Due to the relatively small impact of acidic fluids on the reservoir, the pore types of the reservoir are mainly primary pores with good physical properties.

Keywords: volcanogenic sediment; diagenetic sequence; reservoir quality; the Wenchang Formation; the Enping Formation; Huizhou Sag; Pearl River Mouth Basin

Citation: Chen, J.; Zhu, H.; Peng, G.; Ding, L.; Zeng, Z.; Wang, W.; Tao, W.; Zhou, F. Diagenetic Evolution of Syngenetic Volcanogenic Sediment and Their Influence on Sandstone Reservoir: A Case Study in the Southern Huizhou Sag, Pearl River Mouth Basin, Northern South China Sea. *J. Mar. Sci. Eng.* **2024**, *12*, 1459. https://doi.org/10.3390/jmse12081459

Academic Editor: Timothy S. Collett

Received: 9 July 2024
Revised: 20 August 2024
Accepted: 21 August 2024
Published: 22 August 2024

1. Introduction

With the continuous improvement of exploration, shallow oil and gas exploration can no longer meet the increasing demand for oil and gas. Deep exploration, as one of the important areas of oil and gas energy exploration, has become a hotspot in the global oil and gas geological field [1–4]. However, due to the large burial depth and strong reservoir heterogeneity, it is difficult to predict the distribution of high-quality reservoirs, which also restricts the continuous development of deep oil and gas exploration [5–14]. As an important oil and gas producing area in the Pearl River Mouth Basin (PRMB) of the South China Sea, Huizhou Sag has also shifted its exploration focus to the deep layer in recent years,

and many large-scale oil and gas reservoirs have been found in the deep Paleogene, which proves the deep exploration potential of Huizhou Sag [15–19]. The PRMB of Paleogene was a continental rift basin with strong and complex tectonic activity. The Huizhou Sag also experienced strong tectonic activity in the Paleogene, including the first and second episode of the Zhuqiong movement (about 54 Ma and 39.4 Ma) and the Nanhai movement (about 29.3 Ma), which was also accompanied by many volcanic eruptions [20–24]. Generally, intensive volcanic activity has a significant impact on sedimentation, reservoirs and source rocks, which can alter the sedimentary pattern, the quality of reservoirs and source rocks and the distribution of oil and gas reservoirs [25–36]. The incorporation of a large amount of volcanogenic sediment will lead to more complex and unpredictable reservoir characteristics [34,37,38]. Previous studies have mainly focused on elucidating the characteristics and reservoir-forming mechanisms of deep reservoirs [39–41]. However, there has been little research on the impact mechanism of volcanogenic sediment in areas with intense volcanic activity. Because of the strong impact on the reservoir, evaluating the impact of volcanic activity and volcanogenic sediment in reservoirs and oil and gas reservoirs is an important foundation for predicting high-quality reservoirs in the Huizhou Sag.

Volcanic activity often affects strata in two forms, including volcanic eruption and magma intrusion. Volcanic eruption mainly affects contemporaneous sedimentary layers [42–45]. Volcanic materials are often accompanied by volcanic eruption, mixed with contemporaneous sedimentary debris, and participate in later diagenesis evolution as dissolution components. The intrusion of magma mainly affects the early pre-existing strata. The intrusion of magma will transmit heat to the strata, causing thermal alteration of rock strata and even the recycling of sand bodies [27–29,35,46–60].

In this paper, we studied the characteristics and evolution of volcanogenic sediments in the Wenchang and Enping Formation of Huizhou 26 subsag, Huizhou Sag, Zhu-I Depression, Pearl River Mouth Basin, aiming to (1) define the reservoir characteristics of the Wenchang and Enping Formation; (2) study the characteristics and differences of volcanogenic sediments in different strata; and (3) discuss the diagenetic evolution of volcanogenic sediments and its influence on reservoir characteristics and evolution.

2. Geological Setting

The Pearl River Mouth Basin (PRMB), located in the South China Sea, can be divided into five secondary tectonic units from south to north, which are the Southern Uplift Zone, the Southern Depression Zone (Zhu-II Depression, Chaoshan Depression), the Central Uplift Zone, the Northern Depression Zone (Zhu-I Depression and Zhu-III Depression) and the Northern Uplift Zone. The Zhu-I depression is a large depression developed in the Northern Depression Zone of the PRMB. It is NE-trending, adjacent to the Northern Fault Terrace Zone in the north, the Central Uplift Zone in the south and the Zhu-III Depression in the west. From west to east, five negative structural units are arranged in order: Enping Sag, Xijiang Sag, Huizhou Sag, Lufeng Sag and Hanjiang Sag (Figure 1) [20,23,61–65].

The tectonic evolution of the PRMB can be divided into three stages. (1) Rifting stage: According to the tectonic episode, it can be divided into three stages corresponding to the three tectonic movements of the Shenhu movement, the first and the second episode of the Zhuqiong movement. At this stage, the basin experienced multi-stage rifting and tension, resulting in a NE-trending rift zone composed of grabens or semi-grabens. Among them, the near EW-, NE- and NEE-trending boundary faults and NWW-trending faults in the depression controlled the basic structural pattern of the basin, which corresponded to the development of the Shenhu, Wenchang and Enping Formations [66–70]. (2) Post-rift depression stage: This was an evolution stage accompanied by depression and fracture, including a rift-depression transition sub-stage and a depression quiet sub-stage, mainly corresponding to the Nanhai movement and Baiyun movement, which corresponded to the strata of the Zhujiang Formation, Zhuhai Formation and Hanjiang Formation. The basin underwent regional uplift and denudation in the Late Oligocene and transformed from a rift to a depression. The NWW fault activity was slightly stronger, and the fault

activity in other directions continued to weaken [21,71]. (3) Fault block activity stage: The PRMB experienced block fault rise and fall, and the uplift area suffered different degrees of denudation, frequently fracture and magmatic activity, corresponding to the Dongsha movement (Figure 2) [26,72,73].

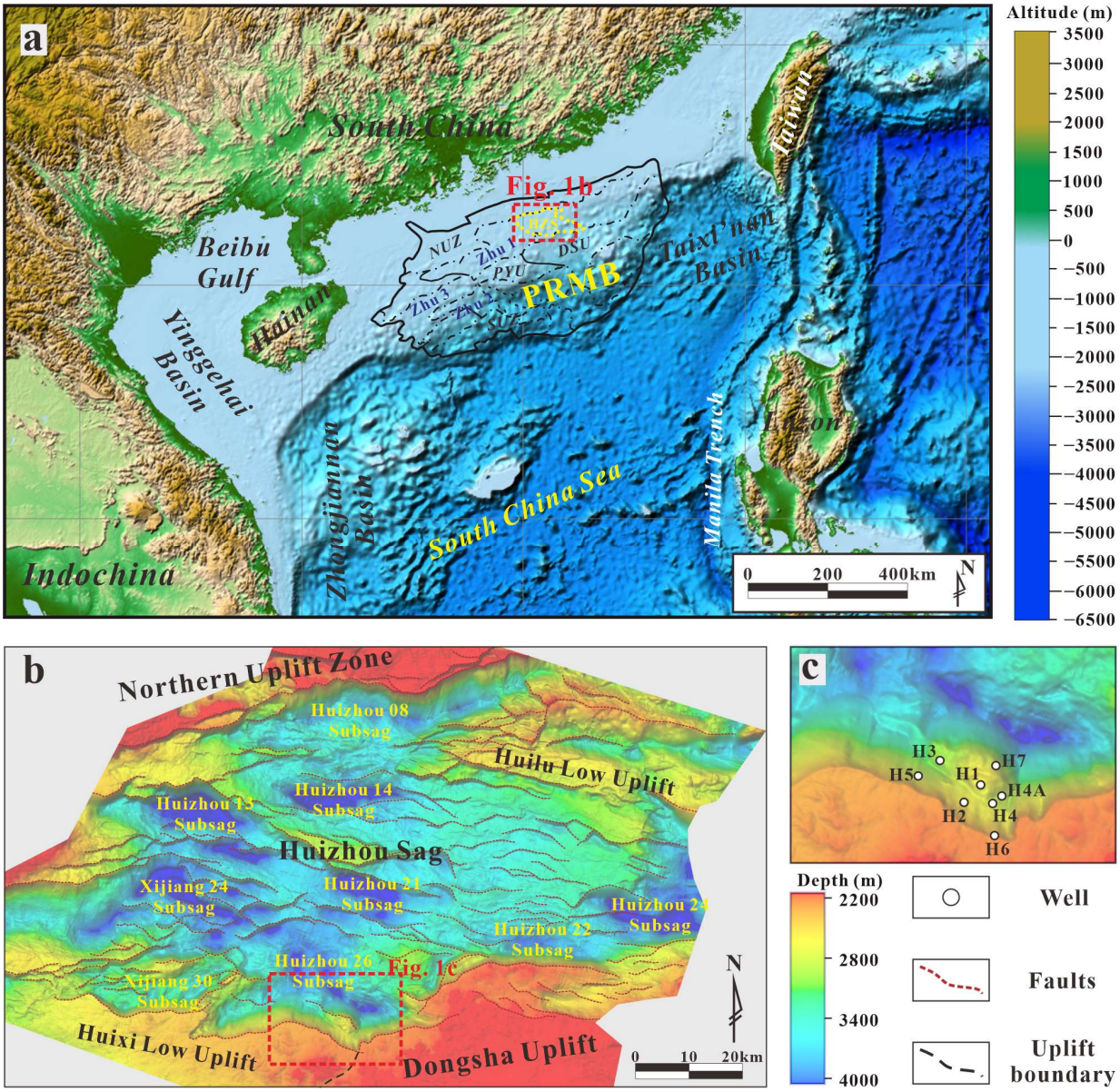

Figure 1. (**a**) Topography and altitude of the South China Sea and adjacent regions with locations of the major sedimentary basins, including the Huizhou Sag (HZS) in Zhu-I Depression. (**b**) Main morphological pattern that penetrated the Wenchang-Enping Formation in Huizhou Sag. (**c**) Main morphological pattern and boreholes in Huizhou 26 Subsag. Abbreviations: PRMB = Pearl River Mouth Basin; Zhu 1 = Zhu-I Depression; Zhu 2 = Zhu-II Depression; Zhu 3 = Zhu-III Depression; NUZ = Northern Uplift Zone; PYU = Panyu Uplift; DSU = Dongsha Uplift; SUZ = Southern Uplift Zone.

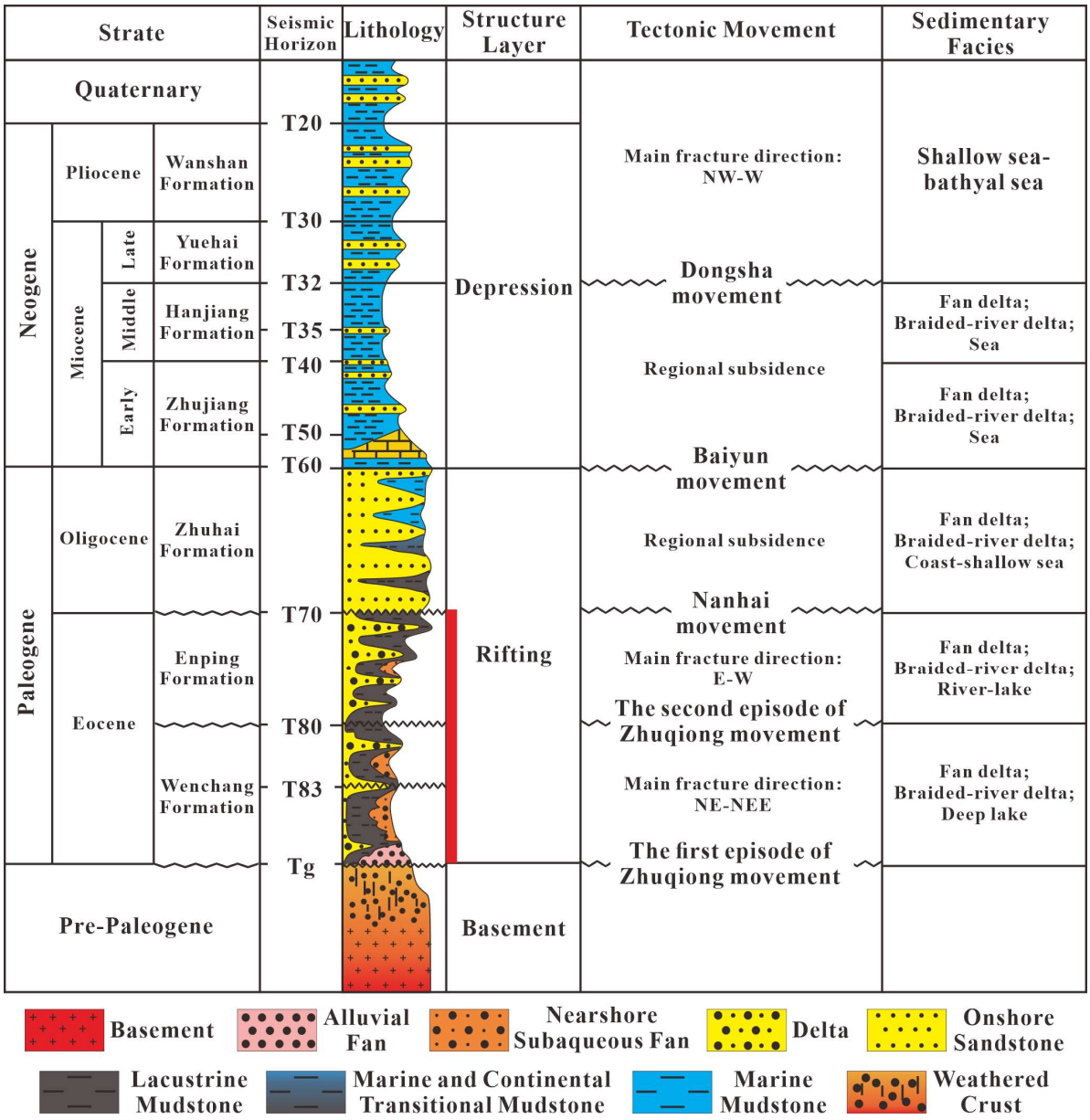

Figure 2. Generalized stratigraphic column of the Huizhou Sag, Pearl River Mouth Basin (modified from [19,66]).

The Huizhou Sag is located in the middle of Zhu-I depression, north of the Northern Fault Terrace, south of the Central Uplift Zone of Dongsha Uplift, adjacent to Huilu Low Uplift and Huixi Low Uplift to the east and west. The study area is located in the southern margin of Huizhou Sag, with an area of 1500 km^2. The early NE-trending depression-controlling faults and the late NW-trending reformation faults are mainly developed in Huizhou Sag. Under their joint control, the Huizhou Sag shows a structural framework of alternating uplift and sag (Figure 1). The main body of the sag can be divided into several small subsags, which are mainly distributed along the depression-controlling faults. With strong tectonic activity in the Wenchang Formation, the main sedimentary facies are the fan delta facies and lacustrine facies. The thick lacustrine mudstone in the center of the sag can be used as a high-quality source rock for the Paleogene. With weakening tectonic activity in the Enping Formation, the main sedimentary facies is converted to the large-area braided-river delta facies, without the development of high-quality lacustrine source rocks [16,73,74].

3. Materials and Methods

A total of 164 thin sections of the Wenchang-Enping Formation from 6 wells' sandtone samples were prepared. In order to identify pores and calcite, all thin sections were impregnated with blue epoxy resin and stained with alizarin red-s solution [75,76]. The quantitative statistics of minerals and pores were observed by polarizing microscope with 400 counting points per thin section, using the Gazzi–Dickinson point-counting method [77–79].

A total of 39 gold-coated samples from 4 wells in the Wenchang-Enping Formation were observed used scanning electron microscope (SEM) to examine the morphologies and spatial relationships of diagenetic minerals. These samples were analyzed with JSM-5500LV scanning electron microscope (JEOL. Ltd., Tokyo, Japan) equipped with a Quantax 400 energy-dispersive X-ray (EDX) spectrometer (Bruker Co. Ltd., Billerica, America) under a beam current of 1.0 to 1.5 nA and an acceleration voltage of 20 kV.

A total of 58 samples from 6 wells in the Wenchang-Enping Formation, which were volcanic glass in the rock layer, were analyzed using an electron probe to determine the main element content characteristics of the volcanogenic sediment. These samples were analyzed with a JXA-8320 Electron probe X-ray microanalyzer (JEOL. Ltd., Tokyo, Japan). The test temperature was 20 °C and the humidity was 43%.

A total of 214 core plug porosity and permeability datapoints from 6 wells in the Wenchang-Enping Formation were collected from the CNOOC to analyze the characteristics of reservoir physical properties. The porosity and permeability of the samples were analyzed according to the standard SY-T 6385-1999 [80] 'The porosity and permeability measurement of core in the net confining stress', using a CMS-300 Overburden Pressure Pore-permeator. The core porosity was measured using helium gas, and the measurement accuracy is 0.5 porosity units. The permeability was calculated using a custom pulse decay permeability meter with helium as the detection gas and using total gas flux measurements.

4. Results

4.1. Lithofacies and Petrography of the Wenchang-Enping Formation

The Wenchang Formation (fan delta facies) is mostly composed of thick sand bodies intercalated with thin layers of mud, with a sand content of 50.5–82.7%. The volcanic breccia is more than 300 m thick, indicating strong volcanic activity. At the same time, the development of volcanic rocks indicates that volcanic activity is dominated by effusive facies and synsedimentary volcanic activity. The Enping Formation (braided-river delta facies) is mostly composed of thin interbedded sand and mudstone, with a sand content of 60.3–77.2%. The development of thin-bedded tuff and tuffaceous sandstone in the Enping Formation indicates that the synsedimentary volcanic activity is dominated by explosive facies and has a relatively weak intensity (Figure 3).

The petrologic characteristics between the Wenchang and Enping Formation are different (Figure 4 and Tables 1 and 2). Due to the strong volcanic activity in the study area, a large amount of tuffaceous matrix developed in the reservoir, which is different from the argillaceous matrix. They are both extremely fine in size, but the tuffaceous matrix often appears as aggregated products with various colors and little or no light reflection. The tuffaceous matrix is unstable at high temperatures, often undergoing devitrification and dissolution, with a first-order gray-white interference color. The argillaceous matrix is mainly composed of clay minerals, which are relatively stable and difficult to undergo dissolution and have a high interference color with star-like distribution, which is a main difference from the tuffaceous matrix [29,34,81,82].

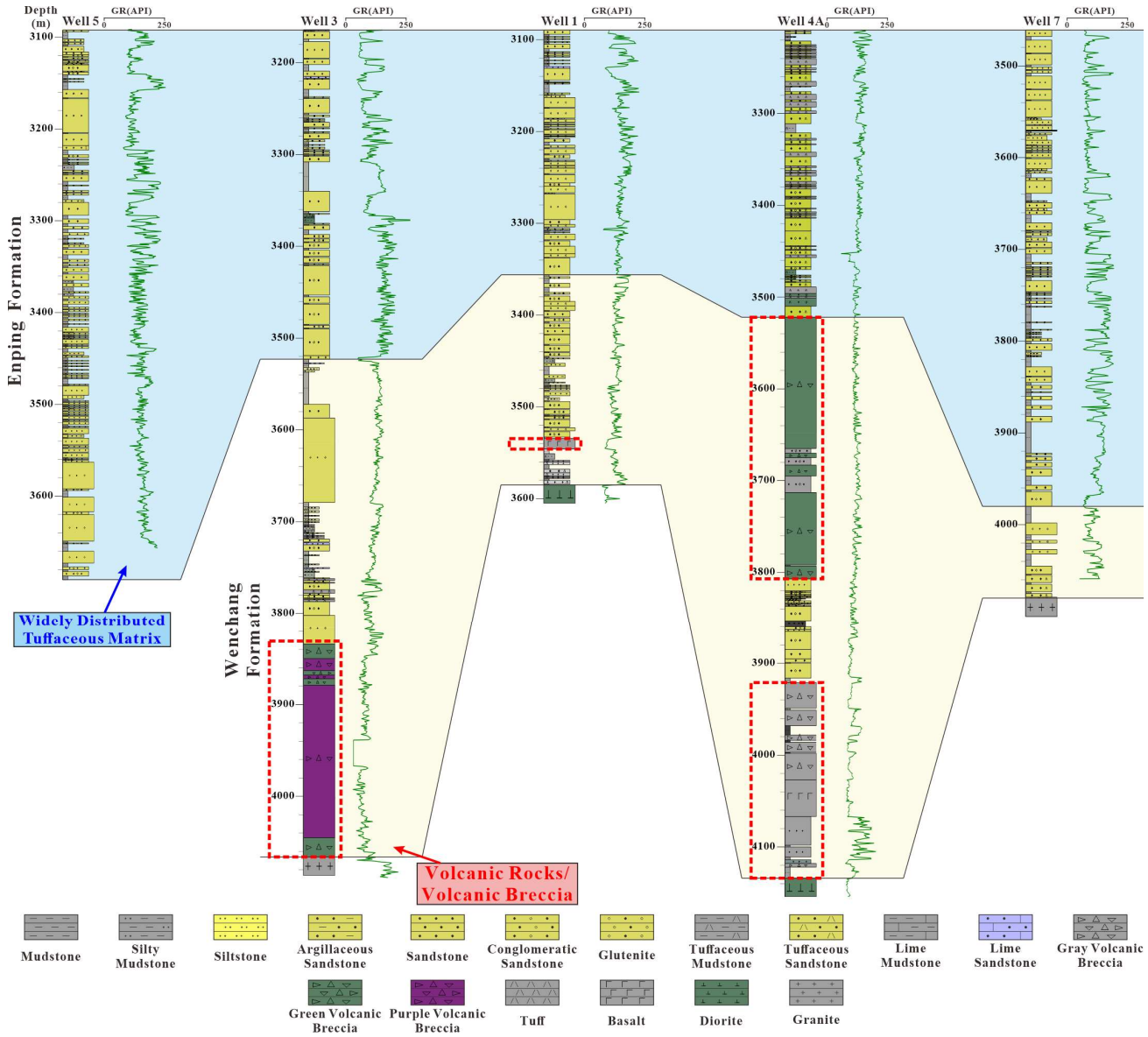

Figure 3. Stratigraphic cross-well sections show the lithologies and GR curve characteristics of the Wenchang-Enping Formation stratum in the Huizhou 26 Subsag. See Figure 1c for the location of the wells. The red box is used to clarify the characteristics of different layers and highlight the location of volcanic rocks and breccias.

Table 1. Content data of component by point count from thin sections.

WELL	DEPTH	STRATA	Q	F	VRF	MRF	SRF	MICA	AM	TM	CC	CM	SC	PY
H1	3158.4	EP	62.0	28.0	6.5	0.0	0.0	3.5	19.0	5.0	0.0	0.0	0.0	0.5
H1	3184	EP	82.5	7.5	9.5	0.5	0.0	0.0	1.0	5.0	22.0	0.5	1.5	0.0
H1	3200	EP	51.0	10.0	38.0	0.0	0.0	1.0	0.0	5.0	0.5	15.0	0.0	2.5
H1	3226	EP	33.5	39.0	24.0	1.0	0.0	2.5	0.0	5.0	0.0	13.0	0.0	0.0
H1	3226	EP	41.0	33.5	25.0	0.0	0.0	0.5	0.0	5.0	0.0	15.0	0.0	0.0
H1	3234.5	EP	36.0	9.0	54.0	0.0	0.0	1.0	0.0	5.0	0.0	5.0	0.0	0.0
H1	3235	EP	31.0	6.0	61.0	0.0	0.0	2.0	0.0	5.0	0.5	0.5	0.0	0.0
H1	3399.4	WC	41.0	11.0	48.0	0.0	0.0	0.0	0.0	10.0	0.0	10.0	0.0	0.0

Table 1. *Cont.*

WELL	DEPTH	STRATA	Q	F	VRF	MRF	SRF	MICA	AM	TM	CC	CM	SC	PY
H1	3503.5	WC	54.0	24.5	21.0	0.0	0.0	0.5	0.0	8.0	0.0	10.0	0.5	0.0
H1	3582	WC	31.0	46.5	22.5	0.0	0.0	0.0	20.0	15.0	0.0	0.0	0.0	0.0
H3	3166.5	EP	79.6	14.0	5.1	0.6	0.6	0.0	0.0	0.0	0.0	0.0	1.0	0.0
H3	3182	EP	73.6	16.0	7.4	0.0	3.1	0.0	0.0	0.0	0.0	0.0	1.0	0.0
H3	3211	EP	79.8	13.1	6.0	1.2	0.0	0.0	0.0	0.0	0.0	0.0	1.0	0.0
H3	3223	EP	64.3	15.5	20.2	0.0	0.0	0.0	0.0	0.0	0.0	0.0	1.0	0.0
H3	3266.5	EP	78.3	12.0	7.8	0.6	1.2	0.0	0.0	0.0	0.0	0.0	1.0	0.0
H3	3281.5	EP	77.8	12.6	5.2	1.5	0.0	3.0	1.0	0.0	0.0	0.5	0.0	0.0
H3	3304	EP	78.1	9.5	10.1	0.0	0.0	2.4	0.0	6.0	1.5	0.0	0.5	0.0
H3	3360	EP	63.9	9.6	23.5	0.0	0.6	2.4	0.0	0.0	0.0	0.0	1.0	0.0
H3	3380	EP	59.5	7.7	27.4	0.0	0.6	4.8	0.0	16.0	0.0	0.0	0.0	0.0
H3	3521	EP	82.1	11.4	5.7	0.0	0.8	0.0	15.0	0.0	0.0	0.0	1.0	0.0
H3	3572.5	WC	54.0	10.4	29.4	0.0	4.9	1.2	0.0	0.0	0.0	0.0	1.0	0.0
H3	3583	WC	74.1	14.5	9.6	0.0	1.2	0.6	0.0	0.0	0.0	0.0	1.0	0.0
H3	3596	WC	56.6	6.0	34.9	0.0	0.0	2.4	0.0	16.0	0.0	0.0	0.0	0.0
H3	3615	WC	60.0	8.2	30.0	0.0	1.8	0.0	0.0	1.0	0.0	0.0	1.0	0.0
H3	3719.5	WC	38.6	4.2	56.6	0.0	0.6	0.0	0.0	2.0	0.0	0.0	0.5	0.0
H3	3726	WC	50.7	23.3	23.3	1.4	1.4	0.0	0.0	16.5	0.5	0.5	1.0	0.0
H3	3791	WC	45.2	7.1	47.6	0.0	0.0	0.0	0.0	0.0	0.0	6.0	0.0	0.0
H3	3794	WC	62.0	12.7	25.3	0.0	0.0	0.0	0.0	10.0	0.0	0.0	0.0	0.0
H3	3798	WC	42.5	11.0	45.2	0.0	1.4	0.0	0.0	0.0	0.0	0.0	0.0	0.0
H3	3801.5	WC	44.9	15.4	38.5	0.0	0.0	1.3	0.0	22.0	0.0	0.0	0.0	0.0
H3	3816.5	WC	63.3	15.2	20.3	0.0	1.3	0.0	0.0	3.0	0.0	0.0	0.0	0.0
H4A	3600	WC	49.4	4.5	46.1	0.0	0.0	0.0	0.0	0.0	0.0	0.0	0.0	0.0
H4A	3705	WC	34.9	10.5	54.7	0.0	0.0	0.0	0.0	6.0	0.0	0.0	0.0	0.0
H4A	3808.5	WC	73.3	12.8	14.0	0.0	0.0	0.0	0.0	12.0	0.0	0.0	0.0	0.0
H4A	3820.15	WC	67.8	12.1	18.4	0.0	0.6	1.1	0.0	12.0	0.0	0.0	0.0	0.0
H4A	3821.4	WC	72.4	8.2	18.8	0.0	0.0	0.6	0.0	12.0	0.0	0.0	0.0	0.0
H4A	3822.97	WC	75.9	8.0	14.9	0.0	0.0	1.1	0.0	11.0	0.0	0.0	0.0	2.0
H4A	3823.5	WC	79.8	8.3	11.9	0.0	0.0	0.0	0.0	10.0	0.0	0.0	0.0	0.0
H4A	3824.45	WC	75.6	9.8	14.6	0.0	0.0	0.0	0.0	0.0	18.0	0.0	0.0	0.0
H4A	3825.41	WC	85.9	9.4	4.7	0.0	0.0	0.0	0.0	12.0	0.0	0.0	0.0	0.0
H4A	3826.19	WC	84.3	10.8	4.8	0.0	0.0	0.0	0.0	9.0	4.0	0.0	0.0	1.5
H4A	3827.5	WC	68.1	15.0	16.3	0.6	0.0	0.0	0.0	15.0	0.0	0.0	5.0	0.0
H4A	3828.12	WC	73.9	12.7	13.4	0.0	0.0	0.0	0.0	12.0	5.0	0.0	0.0	0.0
H4A	3829.43	WC	63.6	16.4	20.0	0.0	0.0	0.0	45.0	0.0	0.0	0.0	0.0	0.0
H4A	3830.86	WC	71.6	14.9	13.5	0.0	0.0	0.0	0.0	0.0	26.0	0.0	0.0	0.0
H4A	3831.96	WC	63.5	21.2	15.3	0.0	0.0	0.0	0.0	13.5	1.0	0.0	0.5	0.0
H4A	3832.93	WC	83.3	11.9	3.6	0.0	0.0	1.2	0.0	12.5	0.0	0.0	0.5	0.0

Table 1. *Cont.*

WELL	DEPTH	STRATA	Q	F	VRF	MRF	SRF	MICA	AM	TM	CC	CM	SC	PY
H4A	3833.68	WC	76.1	11.4	12.5	0.0	0.0	0.0	0.0	12.0	0.0	0.0	0.0	0.0
H4A	3834.59	WC	71.6	6.2	21.0	0.0	0.0	1.2	0.0	19.0	0.0	0.0	0.0	0.0
H4A	3835.45	WC	82.1	8.3	9.5	0.0	0.0	0.0	0.0	12.0	0.0	0.0	0.5	0.0
H4A	3836.7	WC	80.4	7.6	12.0	0.0	0.0	0.0	0.0	14.0	0.0	0.0	0.0	0.0
H4A	3837.43	WC	77.0	9.2	13.8	0.0	0.0	0.0	0.0	10.0	0.0	0.0	0.0	0.0
H4A	3848.5	WC	76.6	14.3	9.1	0.0	0.0	0.0	0.0	12.0	0.0	0.0	0.0	0.0
H4A	3868.3	WC	78.6	11.9	9.5	0.0	0.0	0.0	0.0	11.0	0.0	0.0	0.0	0.0
H4A	3871	WC	69.0	19.0	11.9	0.0	0.0	0.0	16.0	0.0	0.0	0.0	0.0	0.0
H4A	3873.6	WC	76.5	12.3	11.1	0.0	0.0	0.0	0.0	5.0	0.0	0.0	0.0	0.0
H4A	3879	WC	75.9	16.5	7.6	0.0	0.0	0.0	0.0	5.0	0.0	0.0	0.0	0.0
H4A	3883.3	WC	76.1	9.1	14.8	0.0	0.0	0.0	0.0	7.5	0.0	0.0	0.5	0.0
H4A	3886.5	WC	73.9	10.2	15.9	0.0	0.0	0.0	0.0	11.0	0.5	0.0	0.0	0.0
H4A	3897	WC	76.2	16.7	7.1	0.0	0.0	0.0	0.0	12.0	0.0	0.0	0.0	0.0
H4A	3907.5	WC	68.3	13.4	18.3	0.0	0.0	0.0	0.0	10.0	0.0	0.0	0.0	0.0
H4A	3912.5	WC	57.6	5.9	10.6	0.0	25.9	0.0	0.0	10.0	0.0	0.0	0.0	0.0
H4A	4082	WC	73.6	10.3	16.1	0.0	0.0	0.0	0.0	6.0	0.0	0.0	0.0	0.0
H4A	4094	WC	49.7	10.1	40.2	0.0	0.0	0.0	0.0	15.0	0.0	0.0	0.0	0.0
H4A	4109	WC	46.4	8.3	45.2	0.0	0.0	0.0	0.0	13.5	0.0	0.0	0.0	0.0
H5	3113.8	EP	74.5	17.5	4.0	4.0	0.0	0.0	7.0	2.0	0.0	0.0	1.5	0.5
H5	3120.47	EP	79.5	16.5	3.5	0.5	0.0	0.0	3.0	2.0	0.0	0.0	0.5	1.0
H5	3125.15	EP	77.0	9.0	6.0	5.0	1.0	2.0	4.0	5.0	0.0	1.5	0.0	0.5
H5	3134.42	EP	71.5	17.5	6.5	4.0	0.0	0.5	1.0	3.0	0.0	0.0	0.5	1.0
H5	3136.41	EP	73.0	17.0	8.0	2.0	0.0	0.0	0.0	5.0	3.0	0.0	1.5	0.0
H5	3160	EP	74.5	18.0	5.5	1.5	0.5	0.0	4.5	5.0	0.0	1.5	2.0	0.0
H5	3186.5	EP	76.5	15.5	7.0	0.5	0.5	0.0	0.0	5.0	0.0	0.0	2.0	0.0
H5	3195	EP	68.0	21.5	4.0	6.0	0.0	0.5	0.0	5.0	0.0	0.0	2.0	0.0
H5	3206	EP	79.0	5.0	16.0	0.0	0.0	0.0	3.5	15.0	0.0	9.0	0.5	1.0
H5	3284	EP	77.0	17.0	6.0	0.0	0.0	0.0	0.0	5.0	0.0	0.0	1.0	0.0
H5	3288	EP	76.0	18.0	5.0	0.0	1.0	0.0	0.0	5.0	0.0	0.0	1.5	0.0
H5	3314	EP	74.0	11.5	7.0	5.5	1.0	1.0	7.0	15.0	0.0	0.0	2.0	0.5
H5	3421	EP	70.5	16.5	8.5	4.0	0.5	0.0	1.0	10.0	0.0	12.0	2.0	0.5
H5	3425	EP	75.0	14.5	9.0	0.0	1.5	0.0	0.0	5.0	6.0	5.5	1.0	0.5
H5	3429.5	EP	79.5	14.0	5.5	1.0	0.0	0.0	1.0	10.0	1.5	3.5	3.0	1.0
H5	3433.6	EP	74.5	16.5	6.5	2.5	0.0	0.0	1.5	15.0	0.0	7.0	2.0	0.0
H5	3524.6	EP	73.5	14.5	9.5	0.0	0.0	2.5	17.0	20.0	0.0	0.0	0.0	0.0
H5	3553	EP	74.5	14.5	6.0	0.5	0.0	4.5	18.0	22.0	0.0	0.0	0.0	0.0
H5	3554.5	EP	80.0	15.5	3.0	0.0	0.5	1.0	7.0	5.0	1.0	1.0	0.5	0.0
H5	3581	EP	79.5	16.0	3.5	0.5	0.5	0.0	0.0	5.0	1.0	0.5	4.0	0.0
H7	3462	EP	73.5	18.5	4.0	3.0	0.5	0.5	0.0	0.0	0.0	0.0	2.0	0.0
H7	3480	EP	72.5	19.0	2.0	4.5	1.0	1.0	1.0	0.0	0.0	0.0	2.0	0.0

Table 1. *Cont.*

WELL	DEPTH	STRATA	Q	F	VRF	MRF	SRF	MICA	AM	TM	CC	CM	SC	PY
H7	3514	EP	77.5	14.5	5.0	3.0	0.0	0.0	0.0	0.0	0.0	0.0	2.0	0.0
H7	3632	EP	70.5	21.0	3.5	4.0	0.5	0.5	1.0	0.0	0.0	0.5	1.0	0.5
H7	3649.5	EP	65.5	24.0	6.0	4.0	0.0	0.5	1.0	1.0	0.0	0.5	1.5	0.0
H7	3660	EP	79.0	4.5	5.5	10.5	0.0	0.5	0.0	2.0	0.0	0.0	0.5	0.0
H7	3672.5	EP	68.0	23.5	7.5	1.0	0.0	0.0	1.5	0.0	0.0	0.0	3.0	1.5
H7	3676.5	EP	68.0	24.0	4.5	3.0	0.0	0.5	9.0	0.0	0.5	0.5	3.0	0.0
H7	3684	EP	54.0	21.0	12.0	12.5	0.0	0.5	17.0	0.0	0.0	0.5	1.5	0.5
H7	3690.3	EP	84.0	5.5	3.5	6.0	0.0	1.0	0.0	0.5	0.0	1.5	2.0	0.0
H7	3700	EP	67.0	20.5	9.0	3.5	0.0	0.0	0.0	0.0	0.3	0.2	3.0	0.0
H7	3715	EP	78.0	9.5	12.0	0.5	0.0	0.0	3.0	1.0	0.0	3.0	0.5	0.0
H7	3721.5	EP	69.5	20.5	6.0	3.5	0.0	0.5	1.0	0.0	0.0	0.0	2.0	0.5
H7	3738	EP	67.5	26.5	3.0	1.0	0.0	2.0	1.0	1.0	0.0	5.0	1.0	0.0
H7	3743	EP	63.0	23.5	6.0	5.5	0.0	2.0	3.5	0.0	0.5	0.5	3.0	1.0
H7	3758	EP	67.5	25.5	2.0	1.0	0.0	4.0	0.5	3.0	0.0	3.0	1.0	0.5
H7	3807	EP	64.0	22.0	6.5	5.5	0.0	2.0	1.0	1.0	0.0	4.0	1.0	0.5
H7	3835	EP	67.0	22.0	6.0	4.5	0.0	0.5	3.0	1.0	9.0	0.0	0.5	0.0
H7	3842	EP	64.5	24.0	0.5	3.5	0.0	7.5	0.5	1.5	0.0	2.5	0.5	0.5
H7	3969	EP	53.0	14.0	4.5	25.5	0.0	3.0	16.0	0.5	1.5	0.0	0.0	0.0
H7	3974	EP	65.5	16.5	7.5	9.5	0.0	1.0	0.0	0.0	15.0	0.0	0.0	0.0
H7	4001	WC	63.0	26.0	4.5	6.5	0.0	0.0	0.0	11.0	7.5	0.0	0.0	0.5
H7	4029.4	WC	70.5	17.0	6.5	3.5	2.0	0.5	7.0	6.5	0.5	0.0	1.0	0.0
H7	4051	WC	67.0	15.0	5.5	11.5	0.0	1.0	0.5	6.5	2.5	0.0	0.0	0.0

Note: Q—Quartz; F—Feldspar; VRF—Volcanic rock fragment; MRF—Metamorphic rock fragment; SRF—Sedimentary rock fragment; MICA—Mica; AM—Argillaceous matrix; TM—Tuffaceous matrix; CC—Carbonate cement; CM—Clay mineral; SC—Siliceous cement; PY—Pyrite; EP—Enping Formation; WC—Wenchang Formation. The content of Q, F, VRF, MRF, SRF and MICA is the percentage of all framework grains, the content of AM, TM, CC, CM, SC and PY is the percentage of the entire sample, and the unit is %.

Table 2. Content of component and pores by recalculated parameters from thin sections and porosity and permeability by core analysis in the Wenchang and Enping Formations.

Component, Pore, Porosity and Permeability	Enping Formation		Wenchang Formation	
	Range	Average	Range	Average
Quartz/%	31.0−84.0	69.3	31.0−85.9	65.2
Feldspar/%	4.5−39.0	16.6	4.2−46.5	12.9
Volcanic rock fragment/%	0.5−61.0	10.0	3.6−56.6	20.4
Metamorphic rock fragment/%	0.0−25.5	2.7	0.0−11.5	0.5
Sedimentary rock fragment/%	0.0−3.1	0.3	0.0−25.9	0.8
Mica/%	0.0−7.5	1.1	0.0−2.4	0.2
Argillaceous matrix/%	0.0−19.0	3.0	0.0−45.5	1.7
Tuffaceous matrix/%	0.0−22.0	4.0	0.0−22.0	8.8
Carbonate cement/%	0.0−22.0	1.1	0.0−26.0	1.3
Clay mineral/%	0.0−15.0	1.9	0.0−10.0	0.5

Table 2. *Cont.*

Component, Pore, Porosity and Permeability	Enping Formation		Wenchang Formation	
	Range	Average	Range	Average
Siliceous cement/%	0.0−4.0	1.2	0.0−5.0	0.3
Pyrite/%	0.0−2.5	0.3	0.0−2.0	0.1
Primary pore/%	0.0−40.0	5.7	0.0−24.0	1.9
Interparticle pore/%	0.0−4.5	0.2	0.0−14.0	1.9
Intragranular pore/%	0.0−2.5	0.6	0.0−8.0	1.3
Intercrystalline pore/%	0.0−2.0	0.2	0.0−0.5	0.0
Microfracture/%	0.0−0.1	0.0	0.0−4.0	0.1
Porosity/%	1.5−18.7	11.3	1.2−20.5	11.1
Permeability/mD	0.01−4119.7	297.3	0.01−411.0	12.7

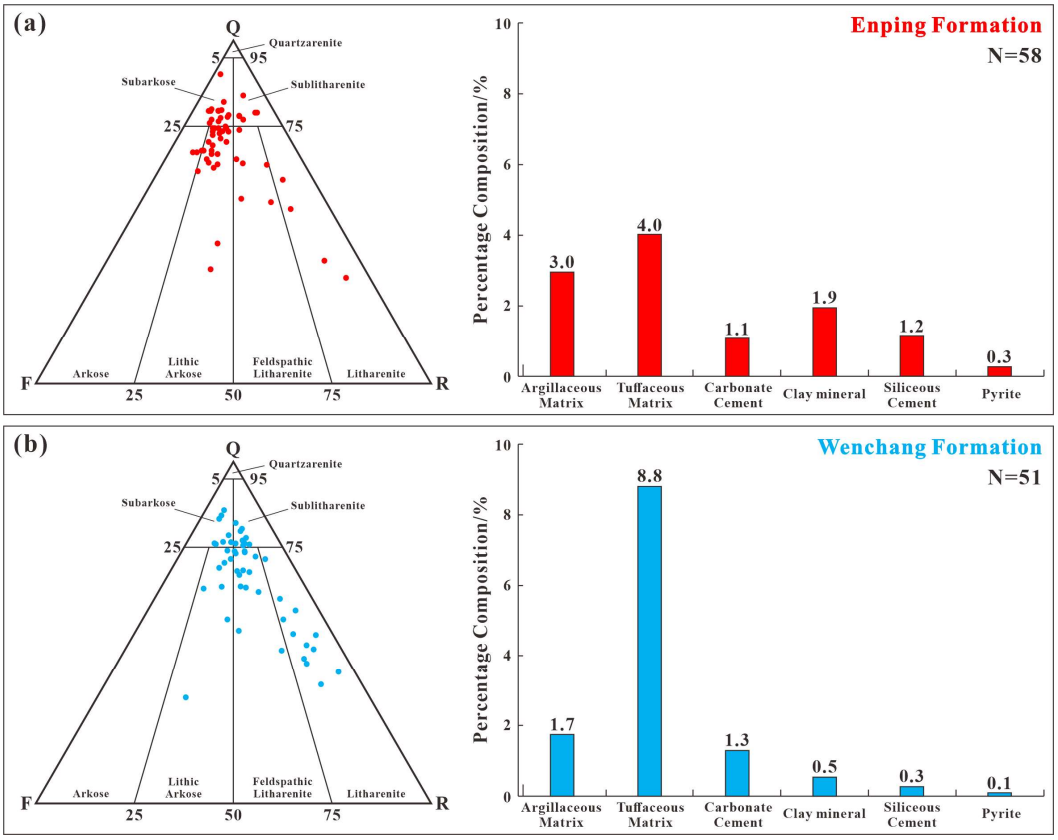

Figure 4. Ternary diagram of rock composition and histogram of the filling material show the composition of the detrital grains and interstitial materials (**a**) for The Enping Formation and (**b**) for the Wenchang Formation (Q, quartz grain; F, feldspar grain; R, rock fragment; modified after [83,84]).

The lithology of Wenchang Formation is dominated by litharenite and feldspathic litharenite. Based on the point-count data, the content of quartz ranges from 31.0% to 85.9% (av. of 65.2%), and the content of feldspar ranges from 4.2% to 46.5% (av. of 12.9%). The rock fragments predominantly consist of volcanic rock fragments (range: 3.6–56.6%; av. of 20.4%), minor metamorphic rock fragments (range: 0.0–11.5%; av. of 0.5%) and minor sedimentary rock fragments (range: 0.0–25.9%; av. of 0.8%). The interstitial materials predominantly consist of tuffaceous matrix (range: 0.0–22.0%; av. of 8.8%), argillaceous matrix (range: 0.0–45.5%; av. of 1.7%), carbonate (range: 0.0–26.0%; av. of 1.3%), minor clay

mineral (range: 0.0–10.0%; av. of 0.5%), minor siliceous cement (range: 0.0–5.0%; av. of 0.3%) and minor pyrite (range: 0.0–2.0%; av. of 0.1%).

The lithology of the Enping Formation is dominated by lithic arkose and subarkose. The content of quartz ranges from 31.0% to 84.0% (av. of 69.3%), and the content of feldspar ranges from 4.5% to 39.0% (av. of 16.6%). The rock fragments predominantly consist of volcanic rock fragments (range: 0.5–61.0%; av. of 10.0%), minor metamorphic rock fragments (range: 0.0–25.5%; av. of 2.7%) and minor sedimentary rock fragments (range: 0.0–3.1%; av. of 0.3%). The interstitial materials predominantly consist of tuffaceous matrix (range: 0.0–22.0%; av. of 4.0%), argillaceous matrix (range: 0.0–19.0%; av. of 3.0%), clay minerals (range: 0.0–15.0%; av. of 1.9%), siliceous cement (range: 0.0–4.0%; av. of 1.2%), minor carbonate (range: 0.0–22.0%; av. of 1.1%) and minor pyrite (range: 0.0–2.5%; av. of 0.3%).

4.2. Diagenetic Events

4.2.1. Compaction

The compaction effect of the HZ26 subsag reservoir is obviously strong, in which the contact mode between the particles changes, the plastic particles deform (mica), the rigid particles (quartz and feldspar) break up to form cracks and the particles are oriented by the compaction effect (Figure 5a–c). The Enping Formation strata, with shallow burial depth and relatively low interstitial content, has a strong anti-compaction ability and a relatively weak compaction effect.

4.2.2. Cementation

- Carbonate Cementation

Carbonate cements are one of the main types of cements, of which calcite is the most common carbonate cement in the Wenchang and Enping Formations (Figure 5d). In the reservoir, the intergranular pores in the areas with strong carbonate cementation are greatly reduced, resulting in poor physical properties. In the areas with moderate or weak carbonate cementation, some residual primary pores are still retained, and these currently exhibit good physical properties. In reservoirs with low matrix content, the content of carbonate cements directly affects the physical properties of the reservoirs.

- Clay Mineral Cementation

Through a large number of rock slices and SEM observation, the clay mineral cements are mainly authigenic kaolinite, chlorite, illite and I/S (Figure 5e–g). The authigenic kaolinite is fibrous, radial or scaly, filled inside the intergranular pores under the microscope and is pseudohexagonal under the scanning electron microscope. The chlorite and illite are flaky or acicular (Figure 5f), and the I/S of the mixed layer is honeycomb and filamentous (Figure 5g). The dissolution of feldspar grains is generally strong in the well section where kaolinite cement appears, and it is speculated that kaolinite may be the product of feldspar dissolution.

- Siliceous Cementation

Siliceous cements are mainly quartz overgrowth and authigenic quartz filling (Figure 5h). The phenomenon of quartz overgrowth is widespread, and the degree of overgrowth is high, and two episodes can be seen. In general, the increase of quartz mostly occurs in the reservoir with temperatures greater than 60 °C, indicating that the buried depth was more than 2000 m [85–89].

- Pyrite Cementation

Pyrite is a relatively low-content cement in the study area, with limited development and only observable in some thin sections. Pyrite is an opaque mineral, so it does not show light under plane-polarized light and cross-polarized light, and it can be seen with a distinct metallic luster under reflected light (Figure 5i). Under the optical microscope, it appears as a clot-like aggregate filling the pores, and the framboidal pyrite can be observed under the SEM (Figure 5i,j).

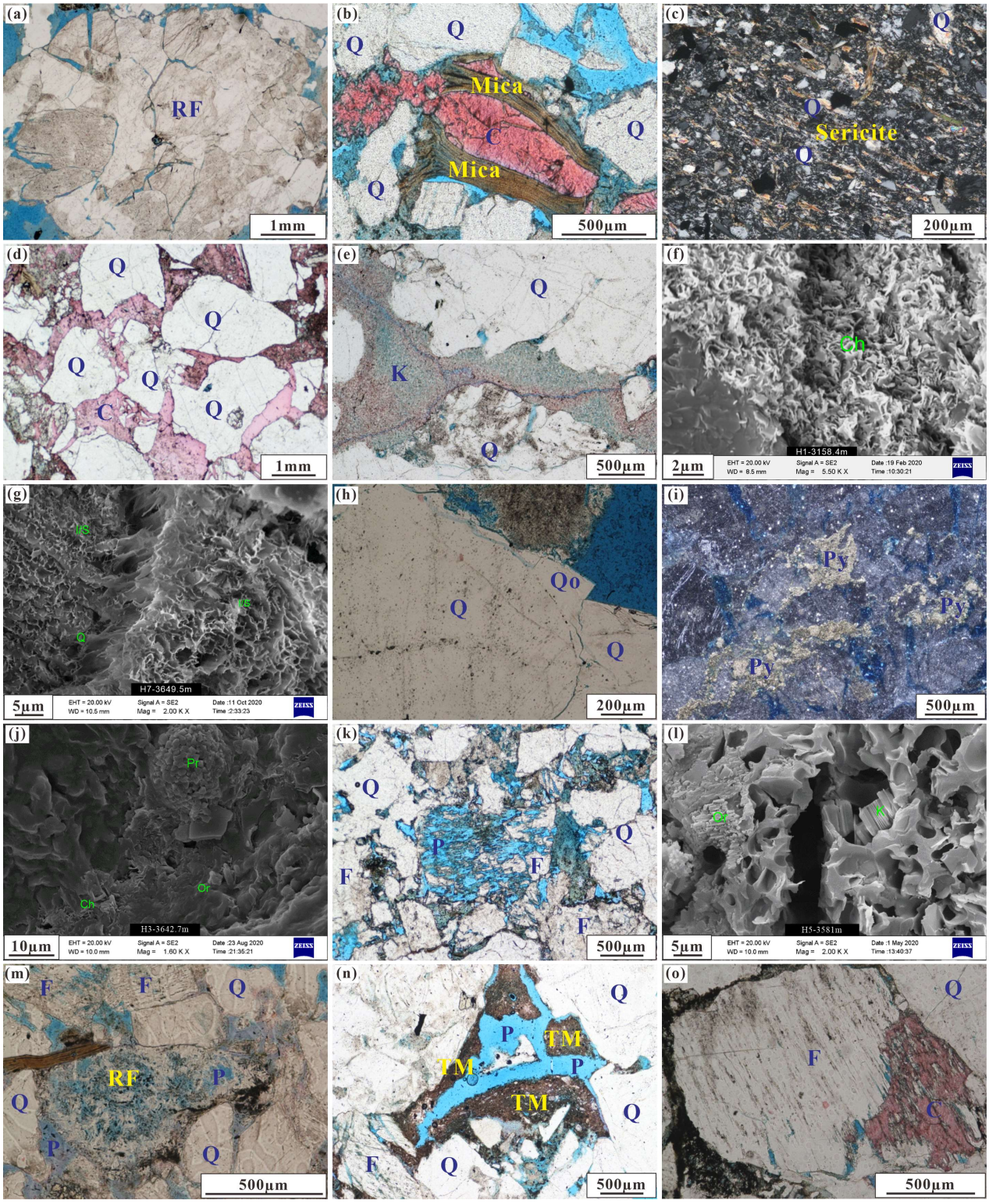

Figure 5. Microscopic characteristics of Paleogene sandstone diagenesis in the Huizhou Sag. (**a**) Fractured rock fragment affected by compaction. Well H1, Wenchang Formation, 3521.5 m, PPL. (**b**) Bended mica affected by compaction. Well H1, Enping Formation, 3235.0 m, PPL. (**c**) Scaly sericites are Oriented distributed by compaction. Well H2, Enping Formation, 3033 m, XPL. (**d**) Carbonate cements in the pore spaces. Well H1, Enping Formation, 3184 m, PPL. (**e**) Kaolinite filled in original pores. Well H5, Enping Formation, 3368.8 m, PPL. (**f**) Acicular kaolinite filled in pores. Well H1, Enping Formation, 3158.4 m, SEM. (**g**) Honeycomb I/S of the mixed layer filled in pores. Well H7,

Enping Formation, 3649.5 m, SEM. (**h**) Quartz overgrowth often develops around quartz grains. Well H5, Enping Formation, 3206 m, PPL. (**i**) The clot-like pyrite filling the pores. Well H3, Enping Formation, 3191 m, RL. (**j**) The framboidal pyrite filling the pores. Well H3, Wenchang Formation, 3642.7 m, SEM. (**k**) Feldspars form secondary dissolution pores along cleavage. Well H1, Enping Formation, 3235 m, PPL. (**l**) Kaolinite filled in the feldspar-dissolved pores. Well H5, Enping Formation, 3581 m, SEM. (**m**) Volcanic rock fragments are dissolved to form secondary pores. Well H1, Wenchang Formation, 3399.4 m, PPL. (**n**) Tuffaceous matrix is dissolved to form interparticle dissolved pores. Well H3, Enping Formation, 3191 m, PPL. (**o**) Carbonate cements replace feldspars, and both dissolve to form secondary pores. Well H5, Enping Formation, 3554.5 m, PPL. Abbreviations: Q, Quartz; Qo, Quartz overgrowth; F, Feldspars; RF, Rock fragment; TM, tuffaceous matrix; C, Carbonate cements; K, Kaolinite; Py, Pyrite; P, Pores; PPL, Plane-polarized light; XPL, Cross-polarized light; RL, Reflected light; SEM, scanning electron microscopy.

4.2.3. Dissolution

The dissolution of particle components and cements is more common; the most common is the dissolution of feldspar particles (Figure 5k,l), followed by the dissolution of coarse-grained volcanic rock debris (Figure 5m) and fine-grained tuffaceous matrix (Figure 5n).

Based on the data of thin sections, the main dissolved pore types of the reservoir are the intragranular pores and interparticle pores. The feldspar composition of the Wenchang Formation reservoir is high, which is more prone to acid dissolution to form secondary pores and improve reservoir properties [40,90,91]. The statistical results of thin sections show that feldspar dissolution is the most intense in dissolution, and the feldspar dissolution pore is the most important part of secondary pores. The K^+, Al^{3+} and SiO_4^{2-} produced by feldspar dissolution are deposited in the form of kaolinite and SiO_2 under appropriate conditions, which provides a material source for quartz overgrowth and authigenic kaolinite [5,85,88,89].

In addition, it is also common that the latest cements are filled in early dissolution pores, such as the dissolution pores of feldspar, which are filled by carbonate cements (Figure 5o), and a small amount of quartz dissolution secondary pores are filled by carbonate cements.

4.3. Pore Type and Reservoir Physical Property

Due to the different diagenesis intensities, pore types and physical properties between the the Wenchang and Enping Formations are different (Figures 6 and 7).

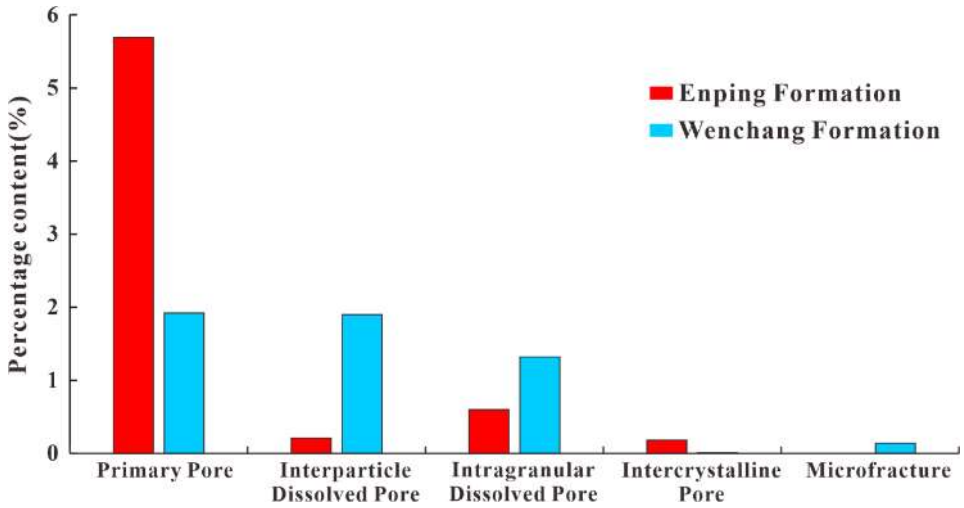

Figure 6. Percentage content histogram of different pore types in the Wenchang and Enping Formations.

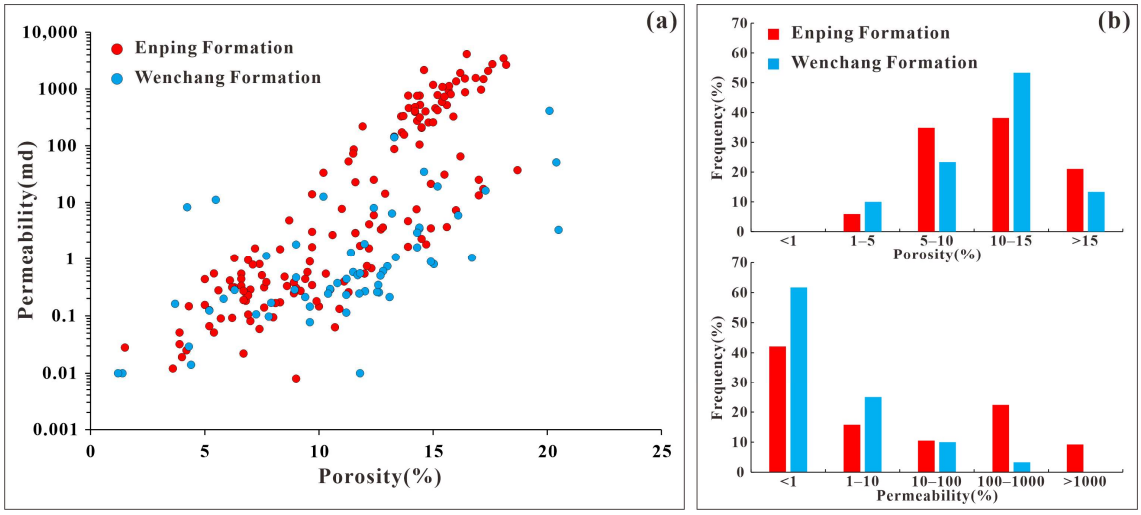

Figure 7. Cross plot (**a**) and frequency distribution histograms of porosity and permeability (**b**) of the Wenchang and Enping Formation reservoirs.

For the Wenchang Formation, the main pore type of sandstones is a secondary dissolved pore, like intergranular and intragranular dissolved pores, mainly formed by the dissolution of feldspar and tuffaceous matrix (smaller than 0.05 mm; in aggregate form; easy to devitrify and dissolve) (Figure 5g,h), with a poor reservoir physical property (porosity: from 1.2% to 20.5%, mean = 11.1%; permeability: from 0.01 mD to 411 mD, mean = 12.7 mD). For the Enping Formation, the main pore type of sandstones is a primary pore; the dissolved pore, like intergranular dissolved pores and intragranular dissolved pores, is relatively low, with a higher reservoir physical property (porosity: from 1.5% to 18.7%, mean = 11.3%; permeability: from 0.01 mD to 4119.7 mD, mean = 294.3 mD). With a similar porosity, the permeability is significantly higher than that of the Wenchang Formation reservoir.

4.4. Characteristic and Differential of Volcanogenic Sediment

Based on drilling cores and thin sections analyses, the Paleogene strata in the Huizhou Sag was strongly affected by volcanic activity, with most wells encountering volcanic rocks (mainly basalt) and pyroclastic rocks (mainly volcanic breccia and tuffaceous sandstone) (Figure 3). The volcanic breccia was produced by volcanic eruptions and is mainly composed of rock fragments (larger than 2 mm) (Figure 8a). Tuffaceous sandstone was mainly composed of terrigenous clasts and volcanic ash (smaller than 2 mm), which had four types pyroclastics: volcanic dust, rock fragments, crystal fragments and vitric fragments [92–94]. Among them, the volcanic dust, which has a particle size less than 0.05 mm, filled the spaces among the crystal fragments, rock fragments and vitric fragments as cements, and was local altered to laumontite (Figure 8b,c). Under cross-polarized light, laumontite is identified by well-developed cleavages and greyish white interference colors (Figure 8b). The SEM images also illustrate that plate-like laumontite crystals fill the pores (Figure 8c). The crystal fragments from the volcanic rock were mainly feldspar and quartz and existed in two forms: angular-subangular and irregular, with concave melting edges (Figure 8d,e). The volcanic rock fragment had typical volcanic rock structures, such as pilotaxitic textures and porphyritic textures (Figure 8f,g). The vitric fragment was uniquely glassy, like chicken-bone and sickle-like (Figure 8h), and was often unstable at low temperatures and prone to devitrification to form felsic textures (Figure 8i) or comb structures [95].

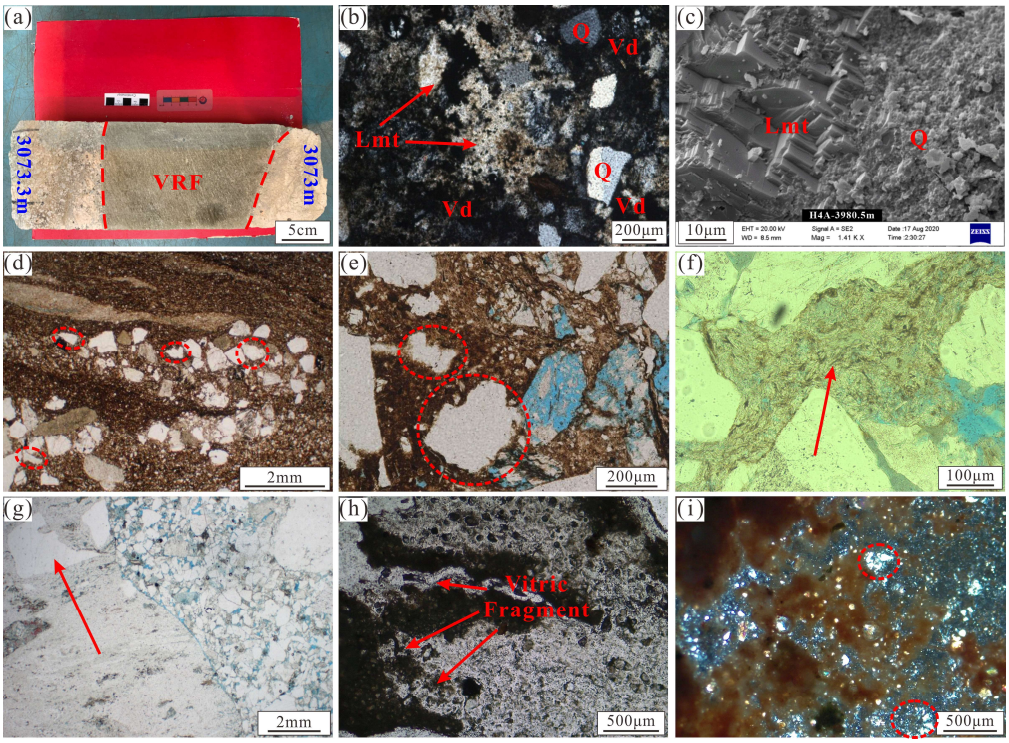

Figure 8. Microscopical identification of volcanic materials. (**a**) Drilling core with volcanic rock fragment (larger than 10 cm). Well H2, Enping Formation, 3073–3073.3 m. (**b**) Volcanic dust filled among crystal fragment and rock fragment, and altered to laumontite (red arrows). Well H4A, Wenchang Formation, 3980.5 m, XPL. (**c**) Plate-like laumontite crystals filling in the pores. Well H4A, Wenchang Formation, 3980.5 m, SEM. (**d**) Angular-subangular feldspar and quartz crystal fragment (red circles). Well H7, Enping Formation, 3943 m, PPL. (**e**) Quartz crystal fragment with concave irregular erosion edge (red circles). Well H7, Wenchang Formation, 4029.4 m, PPL. (**f**) Semiplastic andesite fragment with pilotaxitic texture (red arrow). Well H1, Enping Formation, 3234.5 m, PPL. (**g**) Rhyolite fragment with porphyritic structure, and visible clastic quartz embedded in rhyolite (red arrow). Well H3, Wenchang Formation, 3728.5 m, PPL. (**h**) Chicken-bone and sickle-like volcanic glassy fragment (red arrows). Well H4A, Enping Formation, 3220 m, PPL. (**i**) Volcano glass with felsic texture (red circles). Well H2, Enping Formation, 3165 m, XPL. Abbreviations: Q, Quartz; Vd, Volcanic dust; VRF, Volcanic rock fragment; Lmt, laumontite; PPL, Plane-polarized light; XPL, Cross-polarized light; SEM, scanning electron microscope.

There are significant differences in the characteristics of volcanic materials between the Wenchang and Enping Formations (Figure 3 and Table 3). For the Wenchang Formation, it is dominated by volcanic rocks and volcanic breccias, with relatively high tuffaceous content (mostly higher than 8%) and large particle sizes (mostly greater than 0.2 mm), mostly in the form of skeleton particles. The Enping Formation is dominated by volcanic dust, with relatively low tuffaceous content (mostly less than 8%) and small particle sizes (mostly smaller than 0.2 mm), mostly filling in pores.

Table 3. Tuffaceous content and particle size statistics in the Wenchang and Enping Formations.

Wells	H1	H2	H3	H4A	H5	H7
EP	5.0% (<0.24 mm)	11.6% (<0.2 mm)	2.2% (<0.15 mm)	/	8.2% (<0.35 mm)	0.6% (<0.2 mm)
WC	11.0% (0.3–2 mm)	/	6.4% (0.2–0.5 mm)	9.5% (0.2–1 mm)	/	8% (0.2–0.4 mm)

The geochemical properties of volcanic glass have been analyzed (Figure 9) [96]. For the Wenchang Formation sandstones, the content of SiO_2 ranged from 41.27% to 71.72%, with an average value of 54.78%, and the content of K_2O + Na_2O ranged from 0.05% to

15.51%, with an average value of 4.84%. For the Enping Formation sandstones, the content of SiO_2 ranged from 42.29% to 76.21%, with an average value of 54.76%, and the content of K_2O + Na_2O ranged from 0.21% to 16.88%, with an average value of 5.10%. Combined with the drilled basalt and the andesitic volcanic breccia, the magmatic properties of the Wenchang and Enping Formations were mainly intermediate-basic.

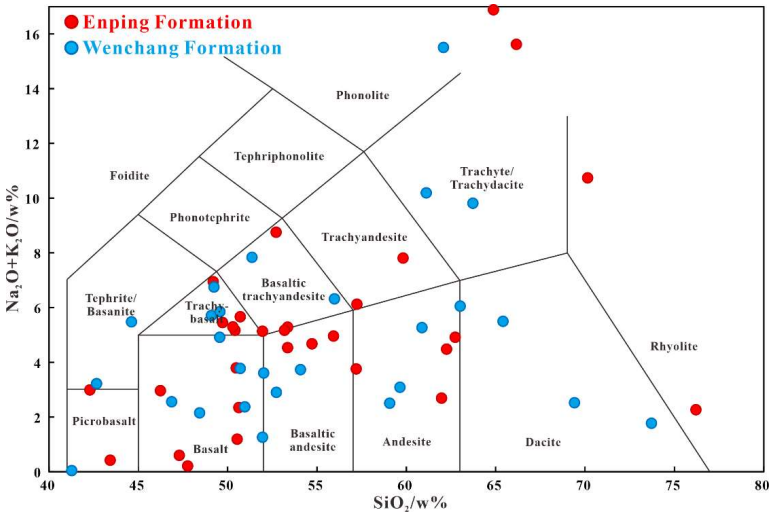

Figure 9. TAS diagram of tuffaceous matter of the Wenchang and Enping Formations [96].

5. Discussion

5.1. Influence of Volcanogenic Sediment on Reservoir

In an area with strong volcanic activity, many volcanic materials entered the reservoir, and their subsequent compaction and alteration had a significant impact on reservoir physical properties [34,37,38].

The types of volcanic materials in the Huizhou Sag were complex: (1) The volcanic dusts had a fine particle size and always filled in the pores as interstitial materials, which could lead to a rapid decline in reservoir physical properties. The reservoir would transform into a tight reservoir (porosity less than 10%, permeability less than 1 mD), while the volcanic dust content was greater than 10% (Figure 10). Although dissolution or alteration might occur later, the improvement of the reservoir was relatively limited. (2) The rock fragment had a relatively coarse particle size and usually existed as skeleton particles, which could enhance the compressive strength of the reservoir. The later dissolution could effectively increase the physical properties of the reservoir, thus having a positive improvement effect on the reservoir. (3) Although the volcanogenic quartz and feldspar fragments had different origins from the terrigenous quartz and feldspar fragments, the same minerals underwent a similar evolution process after the same diagenesis, so they had similar impact on the reservoir and will not be discussed separately. (4) The vitric fragments were formed by pore explosions in magma, with a fine particle size, and were usually plastic. They were easily compacted and deformed later, which could block pores. Although they could cause some degree of dissolution, they would ultimately reduce the physical properties of the reservoir.

With the volcanogenic sediment mixed into the sandstone, the composition of the reservoir has been changed (Tables 1 and 2).

The framework grains of reservoirs in the Wenchang and Enping Formations were both dominated by rigid framework grains (quartz, feldspar and volcanic rock fragments), with a low content of plastic framework grains (mica and vitric fragment; less than 2%) (Tables 1 and 2). Therefore, compaction was difficult for destroying all pores, and its strength was mainly related to burial depth. Subsequent cementation and dissolution also had a significant impact on the reservoir [97].

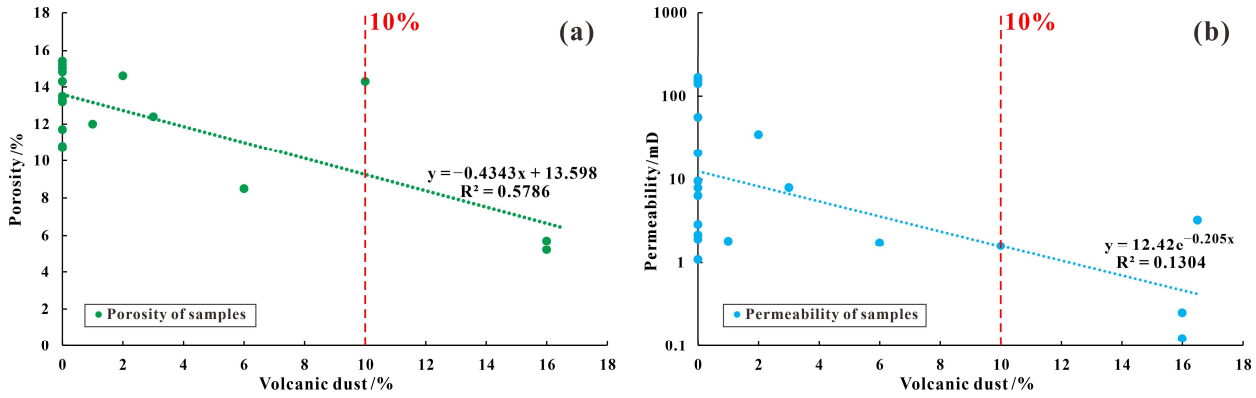

Figure 10. Cross plot of volcanic dust and porosity (**a**) and permeability (**b**) of the Wenchang and Enping Formation reservoirs in Well H3.

The rigid framework grains in the Wenchang Formation were dominated by volcanic frock fragments and feldspar, as well as a large amount of fine-grained tuffaceous matrix filling the pores. The rigid framework grains in the Enping Formation were mainly composed of quartz, with a low content of volcanic rock fragments and tuffaceous matrix due to weak volcanic activity. Because of the different contents of soluble feldspar and volcanic rock debris in different formations, the intensity of dissolution varied, and the types of ions brought by the different components also affected the type and intensity of subsequent cementation [5,34,89].

5.2. Diagenetic Evolution Sequence

According to the indices of organic matter maturity (Ro, %) and petrographic analysis of thin sections and SEM observations, we reconstructed the diagenetic history and defined the diagenetic stage as the mesodiagenetic stage in the study area [91,98–106].

The eodiagenetic stage was mainly characterized by strong compaction and early clay mineral cladding, and the clay minerals were mainly chlorite and C/S mixed-layer. Volcanic dust alteration formed smectite, and it began to become unstable as the burial depth increased. It reacted with the alkaline fluid containing Fe^{2+} and Mg^{2+} produced by the dissolution of volcanic fragment and mica to transform into chlorite and C/S mixed-layer. Authigenic quartz is usually associated with chlorite and develops in areas without chlorite cladding, indicating that early chlorite cladding can inhibit the quartz cementation and protect pores (Figure 11a). At the same time, the evolution and maturity of source rocks released organic acids [82,107–110], which would acid-soluble transform the Paleogene reservoirs, and a large number of feldspar and coarse-grained volcanic fragments would be dissolved (Figure 11b). Al^{3+} and Si^{2+} produced by feldspar corrosion also provided material sources for quartz and kaolinite cementation, so they were generally considered to have formed in the same period. The filling of feldspar dissolution pores by calcite indicated that calcite precipitation occurred after acidic dissolution (Figure 11b,c). Scanning electron microscopy images revealed that the fine-grained volcanic dust mainly underwent alteration, and the alteration products were mainly laumontite and chlorite (Figure 11d). During the mesodiagenetic period, some ankerite cementation (Figure 11e) and late pyrite cementation (Figure 11f) occurred, which made obvious damage to the reservoir.

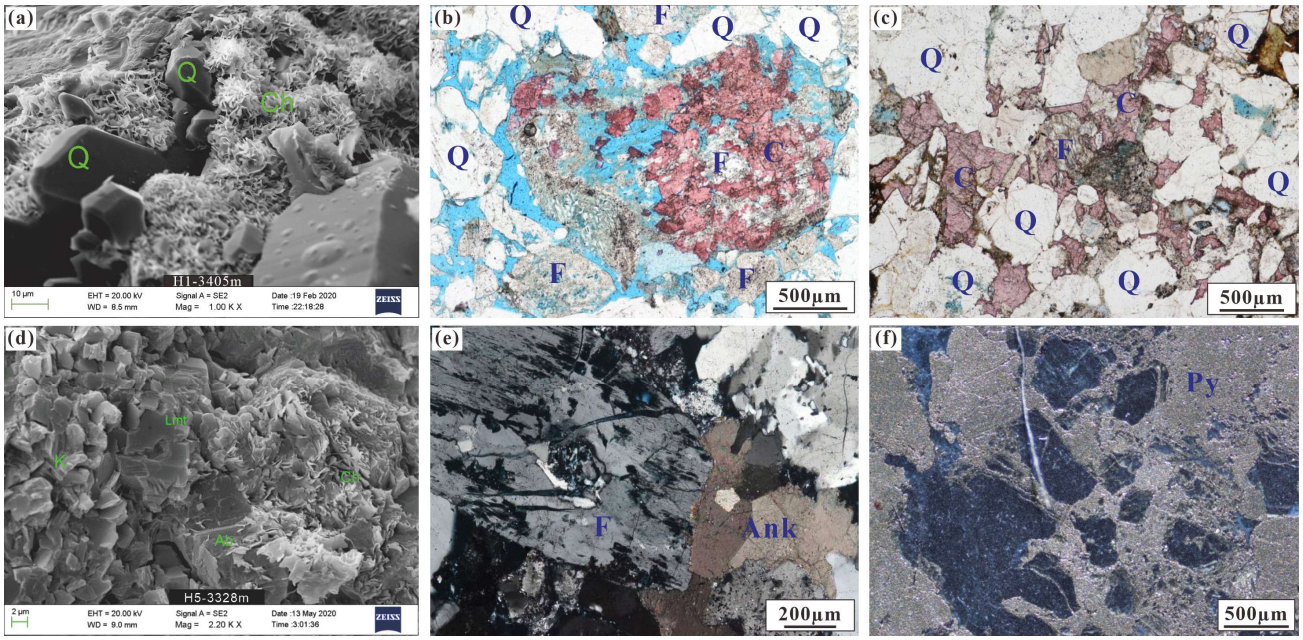

Figure 11. Main diagenetic evolution characteristics. (**a**) Early clay mineral cladding, Well H1, Wenchang Formation, 3405 m, SEM. (**b**) Calcite in feldspar-dissolved pores, Well H3, Wenchang Formation, 3583 m, PPL. (**c**) Calcite in feldspar-dissolved pores, Well H5, Enping Formation, 3429.5 m, PPL. (**d**) Alteration products such as laumontite and clay minerals, Well H5, Enping Formation, 3328 m, SEM. (**e**) Lately ankerite cementation in feldspar-dissolved pores, Well H5, Enping Formation, 3136.41 m, XPL. (**f**) Late pyrite filling residual pores. Well H1, Enping Formation, 3200 m, RL. Abbreviations: Q, Quartz; F, Feldspars; C, Carbonate cements; K, Kaolinite; Ch, chlorite; Ab, Albite; Lmt, Laumontite; Ank, Ankerite; Py, Pyrite; C/S, Mixed-layer chlorite–smectite; P, Pores; PPL, Plane-polarized light; XPL, Cross-polarized light; RL, Reflected light; SEM, scanning electron microscopy.

Therefore, the diagenesis sequence of Huizhou 26 Paleogene reservoir is summarized as follows: (i) compaction, (ii) clay mineral cladding, (iii) feldspar and coarse-grained volcanic fragment dissolution, (iv) kaolinite and quartz cementation, (v) fine-grained tuffaceous alteration, (vi) calcite cementation, (vii) hydrocarbon charge and (viii) late ankerite and pyrite cementation (Figure 12). With higher burial depth and larger content of feldspar and volcanogenic debris sediment, the diagenetic intensity of the Wenchang Formation is significantly higher than that of the Enping Formation [11,17,104]. After complex diagenetic evolution, cements filled the pores, primary pores were destroyed, and dissolution pores developed. Therefore, although the porosity is relatively high, the permeability is significantly lower.

5.3. Formation Mechanism of the Pyroclastic Rock

Volcanic eruptions form volcanogenic sediment, which produces pyroclastic rocks when mixed into terrigenous clasts. The formation and distribution of pyroclastic rocks are related to sedimentary systems and volcanic activities [94,111–113]. The difference of volcanic activity intensity and type will produce different types of volcanogenic sediments and have different effects on sand-bodies and reservoirs (Figure 13).

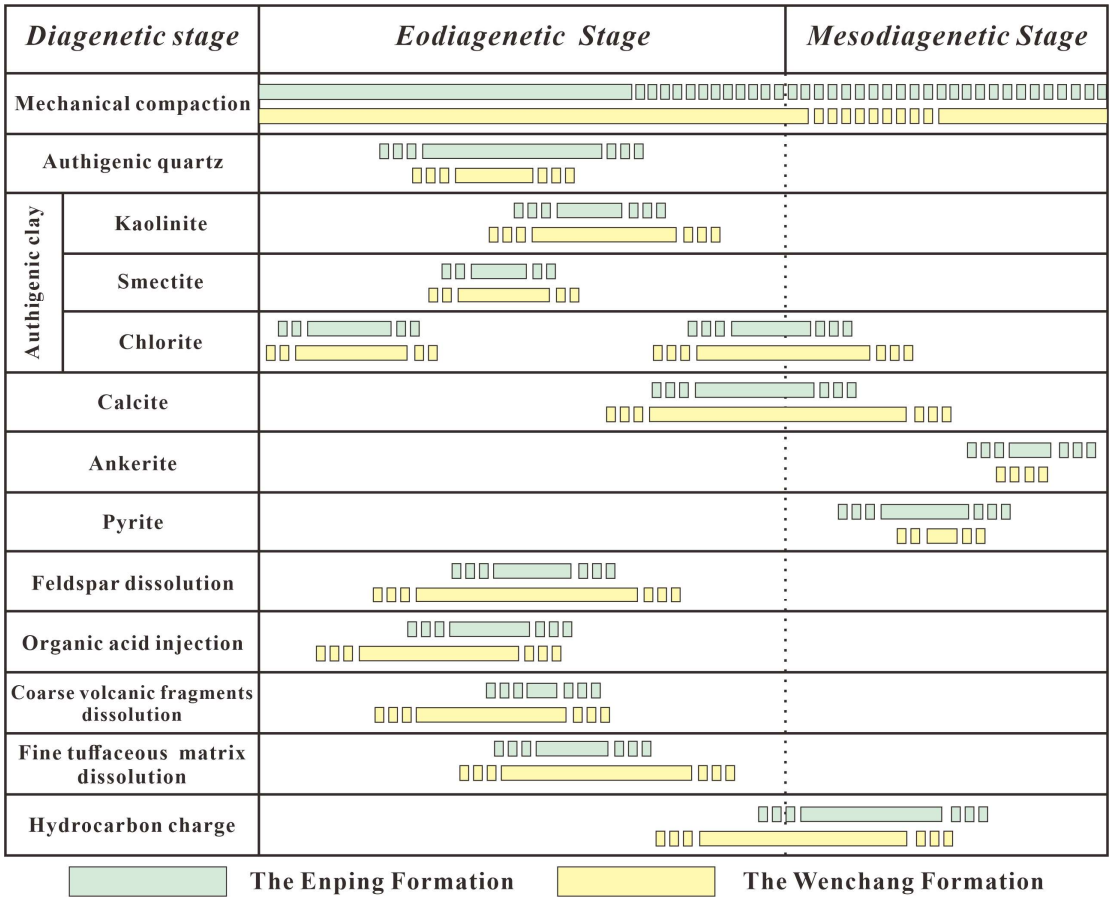

Figure 12. Paragenetic sequence of the diagenetic history of the Wenchang-Enping Formation sandstone reservoirs.

During the period of the Wenchang Formation, the strong tectonic activity led to the large separation of the boundary fault. The type of sedimentary facies was mainly fan-delta, and the short sedimentary distance and weak hydrodynamic conditions led to the low maturity of the reservoir. At the same time, strong tectonic activity led to frequent volcanic activity, and basalt (basic magma) indicated that the volcanic crater was close to the sand body and erupted in the form of effusive. Therefore, many volcanogenic debris sediments mixed into the terrigenous debris, resulting in high content of coarse volcanic rock fragments, and the main type of interstitial materials was fine tuffaceous matrix (volcanic dust). Plastic framework grains and interstitial materials (tuffaceous matrix) led to the weak ability to resist the compaction of the reservoir. Although the early clay mineral cladding was developed, the low content led to the limit impact on the reservoir, so the primary intergranular pores were hard to preserve. With the increase of burial depth, the organic matter began to release organic acid, resulting in the strong dissolution of feldspar and coarse-grained volcanic rock fragments, producing dissolution pores and alteration minerals (kaolinite). With the consumption of acid fluid, the fluid environment changed. In the alkaline environment, carbonate minerals were cemented, fine volcanic dust altered to laumontite and kaolinite reacted with the alkaline fluid containing Fe^{2+} and Mg^{2+} produced by the dissolution of volcanic materials to transform into chlorite. Finally, in the mesodiagenetic stage, local pyrite cements were developed under the influence of hydrothermal fluids. Strong compaction led to the poor preservation of primary intergranular pores in the reservoir, but feldspar and rock fragment dissolution would produce massive secondary dissolved pores. Although carbonate cement and iron cement would fill the pores in the later stage, the impact was relatively limited, so the reservoir porosity is relatively large.

Many interstitial materials and altered secondary minerals blocked pore throats, resulting in the low reservoir permeability.

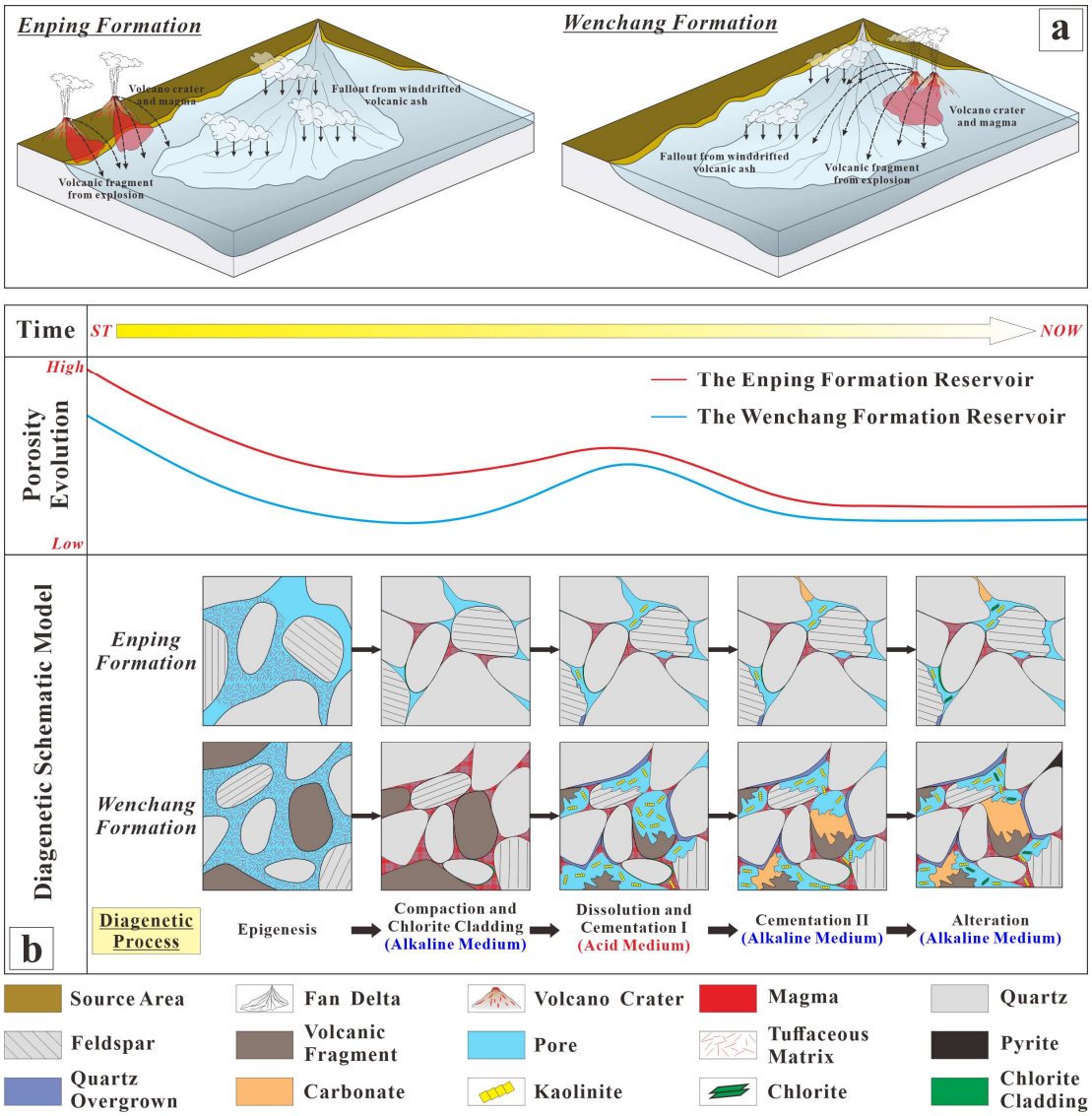

Figure 13. Formation mechanism (**a**) and diagenetic evolution model (**b**) of the Wenchang and Enping Formation pyroclastic rock.

During the period of the Enping Formation, tectonic activity weakened, and the boundary type was mainly a gentle slope boundary. The sedimentary facies changed to braided river delta, and the reservoir maturity increased. The absence of volcanic rock and volcanic breccia indicated that the volcanic activity was weak and far away from the sand body, resulting in fine-grained volcanic dust as the main type of volcanogenic debris sediment in the reservoir. The high content of rigid framework grains (quartz, feldspar) and shallow burial depth resulted in weak compaction effects on the reservoir, allowing for the well-preserved primary intergranular pores. After the entry of acid fluid, feldspar and fine-grained volcanic dust were altered. However, due to the distance from the source rock, the acid fluid could not enter effectively, making it difficult to form dissolution pores, which were mainly altered to produce kaolinite. After the change of the fluid environment, the carbonate minerals were cemented, and kaolinite was transformed into chlorite. The good preservation of primary pores and low interstitial content led to high reservoir porosity and permeability.

6. Conclusions

(1) For the Wenchang Formation, the main lithology is litharenite and feldspathic litharenite, with high content of interstitial material, mainly tuffaceous matrix, and the main pore type is secondary dissolved pores, with an average porosity and permeability of 11.1% and 12.7 mD. For the Enping Formation, the main lithology is lithic arkose and subarkose, with a low content of interstitial materials and complex types. The main pore type is primary pore, with an average porosity and permeability of 11.3% and 294.3 mD.

(2) The magmatic property was mainly intermediate-basic. The types of volcanic materials in the Huizhou Sag were complex. Coarse-grained volcanic fragments could enhance the compressive strength of the reservoir, and the dissolution could effectively increase the physical properties of the reservoir. Fine-grained volcanic dust filled the pores as interstitial materials, resulting in the tightness of the reservoir.

(3) The reservoirs underwent a diagenetic evolution process that was broadly alkaline to acidic and finally alkaline; the diagenesis sequence is summarized as follows: (i) compaction, (ii) clay mineral cladding, (iii) feldspar and coarse-grained volcanic fragment dissolution, (iv) kaolinite and quartz cementation, (v) fine-grained tuffaceous alteration, (vi) calcite cementation, (vii) hydrocarbon charge and (viii) late ankerite and pyrite cementation.

(4) During the period of the Wenchang Formation, strong tectonic activity led to strong volcanic activity, with many volcanic materials mixed into the terrigenous clasts. The rapid sedimentation of the fan delta resulted in lower reservoir maturity and stronger compaction. The dissolution of feldspar and rock fragments generated dissolution pores, increasing porosity, but the clay minerals produced by alteration would block the throat and reduce the reservoir permeability. During the period of the Enping Formation, the volcanic activity was weakened, and the type of volcanic material was mainly fine-grained volcanic dust. The change of sedimentary facies led to the increase of reservoir maturity and weaker compaction. It was difficult for acid fluid to effectively enter the Enping Formation to form dissolution pores, so the content of altered clay minerals was low, resulting in better physical properties.

Author Contributions: Conceptualization, J.C. and H.Z.; methodology, J.C. and H.Z.; validation, J.C., H.Z., Z.Z. and W.W.; formal analysis, J.C.; investigation, G.P., L.D., W.T. and F.Z.; resources, G.P. and L.D.; data curation, J.C., W.T. and F.Z.; writing—original draft preparation, J.C.; writing—review and editing, H.Z., G.P., L.D., Z.Z. and W.W.; visualization, J.C.; supervision, H.Z. and G.P.; project administration, J.C. and H.Z.; funding acquisition, H.Z. and G.P. All authors have read and agreed to the published version of the manuscript.

Funding: This research was funded by the National Natural Science Foundation of China, grant number 41872149 and 41572084.

Institutional Review Board Statement: Not applicable.

Informed Consent Statement: Not applicable.

Data Availability Statement: Data will be made available on request to the corresponding author.

Acknowledgments: The Shenzhen Branch of the China National Offshore Oil Corporation is thanked for providing data used in this study and the permission to publish the results. The State Key Laboratory of Geological Process and Mineral Resources of China University of Geosciences (Wuhan) is thanked for providing the experimental instruments and laboratories for analyzing the major elements in volcanogenic sediments.

Conflicts of Interest: The authors declare that this study received funding from the National Natural Science Foundation of China. The funder was not involved in the study design, collection, analysis, interpretation of data, the writing of this article or the decision to submit it for publication. Authors from the company are only co-authors of this study and has no conflict of interest.

References

1. Xu, S.; Li, S.; Yuan, C. Resource Potential of Water-Soluble Gas in the Palaeogene Huizhou Sag, Pearl River Mouth Basin. *Pet. Explor. Dev.* **2012**, *39*, 194–201. [CrossRef]
2. Yang, C.; Liu, L.; Wu, D.; Jiang, W.; Li, Y.; Xiong, Y. Unscrambling the Source Kitchen and Hydrocarbon Prospect Information of the Ultra-Deepwater Area in Southern Pearl River Mouth Basin, South China Sea: Insights from the First Ultra-Deepwater Exploration Well W21. *J. Pet. Sci. Eng.* **2022**, *216*, 110827. [CrossRef]
3. Cao, H.; Chang, D.; Hu, S.; Zhu, Y.; Wang, Y.; Li, P. Geophysical Techniques and Prospects for Deep Oil-Gas Exploration in China. *Acta Pet. Sin.* **2023**, *44*, 2250–2269.
4. Huang, F.; Wang, S.; Li, M.; Ouyang, J.; Liu, C.; Liu, H.; Zeng, F.; Fan, J.; Jia, P. Progress and Implications of Deep and Ultra-Deep Oil and Gas Exploration in PetroChina. *Nat. Gas Ind.* **2024**, *44*, 86–96.
5. Fu, M.; Song, R.; Xie, Y.; Zhang, S.; Gluyas, J.G. Diagenesis and Reservoir Quality of Overpressured Deep-Water Sandstone Following Inorganic Carbon Dioxide Accumulation: Upper Miocene Huangliu Formation, Yinggehai Basin, South China Sea. *Mar. Pet. Geol.* **2016**, *77*, 954–972. [CrossRef]
6. Wu, D.; Li, H.; Jiang, L.; Hu, S.; Wang, Y.; Zhang, Y.; Liu, Y. Diagenesis and Reservoir Quality in Tight Gas Bearing Sandstones of a Tidally Influenced Fan Delta Deposit: The Oligocene Zhuhai Formation, Western Pearl River Mouth Basin, South China Sea. *Mar. Pet. Geol.* **2019**, *107*, 278–300. [CrossRef]
7. Wu, K.; Xie, X.; Liao, J.; Han, Y. The Rules of Reservoir Characteristics and Dissolution of Paleogene Clastic Rocks in Offshore China. *Earth Sci.* **2023**, *48*, 385–397.
8. Wang, E.; Liu, G.; Pang, X.; Li, C.; Wu, Z. Diagenetic Evolution and Formation Mechanisms of Middle to Deep Clastic Reservoirs in the Nanpu Sag, Bohai Bay Basin, East China. *Pet. Explor. Dev.* **2020**, *47*, 343–356. [CrossRef]
9. Li, Y.; Wu, H.; Zhang, Y.; Liao, Z.; Hu, W.; Fu, H.; Li, Z. Reservoir Diversity and Its Genetic Mechanism in the Es4 Abnormally High-Porosity Zone of Deep Sandstone in the Bonan Step-Fault Zone, Bonan Sag, Bohai Bay Basin, China. *J. Pet. Sci. Eng.* **2020**, *191*, 107216. [CrossRef]
10. Liao, J.; Wu, K.; Er, C. Deep Reservoir Characteristics and Effective Reservoir Control Factors in Baiyun Sag of Pearl River Mouth Basin. *Earth Sci.* **2022**, *47*, 2454–2467.
11. Gong, L.; Gao, X.; Qu, F.; Zhang, Y.; Zhang, G.; Zhu, J. Reservoir Quality and Controlling Mechanism of the Upper Paleogene Fine-Grained Sandstones in Lacustrine Basin in the Hinterlands of Northern Qaidam Basin, NW China. *J. Earth Sci.* **2023**, *34*, 806–823. [CrossRef]
12. Shi, X.; Wu, W.; Hu, H.; Liu, L.; Zhu, Y.; Pan, R.; Meng, J.; Wang, T. The Whole Apertures of Deeply Buried Wufeng-Longmaxi Formation Shale and Their Controlling Factors in Luzhou District, Sichuan Basin. *Earth Sci.* **2023**, *48*, 158–172.
13. Xu, K.; Zhang, H.; Ju, W.; Yin, G.; Wang, H.; Wang, Z.; Wang, Z.; Li, C.; Yuan, F.; Zhao, W. Effective Fracture Distribution and Its Influence on Natural Gas Productivity of Ultra-Deep Reservoir in Bozi-X Block of Kuqa Depression. *Earth Sci.* **2023**, *48*, 2489–2505.
14. Yang, H.; Qian, G.; Xu, C.; Gao, Y.; Kang, R. Sandstone Distribution and Reservoir Characteristics of Shahejie Formation in Huangheko Sag, Bohai Bay Basin. *Earth Sci.* **2023**, *48*, 3068–3080.
15. Jiang, H.; Pang, X.; Chen, D.; Peng, H.; Yu, Q.; Zhang, X. Characteristics of Source Rock Controlling Hydrocarbon Distribution in Huizhou Depression of Pearl River Mouth Basin, South China Sea. *J. Pet. Sci. Eng.* **2018**, *171*, 1260–1268. [CrossRef]
16. Jiang, H.; Pang, X.; Shi, H.; Yu, Q.; Cao, Z.; Yu, R.; Chen, D.; Long, Z.; Jiang, F. Source Rock Characteristics and Hydrocarbon Expulsion Potential of the Middle Eocene Wenchang Formation in the Huizhou Depression, Pearl River Mouth Basin, South China Sea. *Mar. Pet. Geol.* **2015**, *67*, 635–652. [CrossRef]
17. Jin, Z.; Yuan, G.; Zhang, X.; Cao, Y.; Ding, L.; Li, X.; Fu, X. Differences of Tuffaceous Components Dissolution and Their Impact on Physical Properties in Sandstone Reservoirs: A Case Study on Paleogene Wenchang Formation in Huizhou-Lufeng Area, Zhu I Depression, Pearl River Mouth Basin, China. *Pet. Explor. Dev.* **2023**, *50*, 111–124. [CrossRef]
18. Tang, X.; Yu, Y.; Zhang, X.; Peng, G.; Niu, S.; Qiu, X.; Lu, M.; He, Y. Multiphase Faults Activation in the Southwest Huizhou Sag, Pearl River Mouth Basin: Insights from 3D Seismic Data. *Mar. Pet. Geol.* **2023**, *152*, 106257. [CrossRef]
19. Xu, C.; Gao, Y.; Liu, J.; Peng, G.; Liu, P.; Xiong, W.; Song, P. Discovery and Inspiration of Large- and Medium-Sized Glutenite-Rich Oil and Gas Fields in the Eastern South China Sea: An Example from Paleogene Enping Formation in Huizhou 26 Subsag, Pearl River Mouth Basin. *Pet. Explor. Dev.* **2024**, *51*, 15–30. [CrossRef]
20. Xie, H.; Zhou, D.; Li, Y.; Pang, X.; Li, P.; Chen, G.; Li, F.; Cao, J. Cenozoic Tectonic Subsidence in Deepwater Sags in the Pearl River Mouth Basin, Northern South China Sea. *Tectonophysics* **2014**, *615–616*, 182–198. [CrossRef]
21. Ma, B.; Wu, S.; Sun, Q.; Mi, L.; Wang, Z.Z.; Tian, J. The Late Cenozoic Deep-Water Channel System in the Baiyun Sag, Pearl River Mouth Basin: Development and Tectonic Effects. *Deep. Res. Part II Top. Stud. Oceanogr.* **2015**, *122*, 226–239. [CrossRef]
22. He, M.; Zhong, G.; Liu, X.; Liu, L.; Shen, X.; Wu, Z.; Huang, K. Rapid Post-Rift Tectonic Subsidence Events in the Pearl River Mouth Basin, Northern South China Sea Margin. *J. Asian Earth Sci.* **2017**, *147*, 271–283. [CrossRef]
23. Ye, Q.; Mei, L.; Shi, H.; Shu, Y.; Camanni, G.; Wu, J. A Low-Angle Normal Fault and Basement Structures within the Enping Sag, Pearl River Mouth Basin: Insights into Late Mesozoic to Early Cenozoic Tectonic Evolution of the South China Sea Area. *Tectonophysics* **2018**, *731–732*, 1–16. [CrossRef]
24. Wang, X.G.; Zhang, X.; Lin, H.; Que, X.; He, Y.; Jia, L.; Xiao, Z.; Li, M. Paleogene Geological Framework and Tectonic Evolution of the Central Anticlinal Zone in Lufeng 13 Sag, Pearl River Mouth Basin. *Pet. Res.* **2019**, *4*, 238–249. [CrossRef]

25. Zhao, F.; Wu, S.; Sun, Q.; Huuse, M.; Li, W.; Wang, Z. Submarine Volcanic Mounds in the Pearl River Mouth Basin, Northern South China Sea. *Mar. Geol.* **2014**, *355*, 162–172. [CrossRef]
26. Zhang, Z.; Yu, H.; Chen, H.; Du, S.; Li, C. Quantitative Characterization of Fracture-Pore Distribution and Effects on Production Capacity of Weathered Volcanic Crust Reservoirs: Insights from Volcanic Gas Reservoirs of the Dixi Area, Junggar Basin, Western China. *Mar. Pet. Geol.* **2022**, *140*, 105651. [CrossRef]
27. Zhang, S.; Liu, C.; Liang, H.; Jia, L.; Bai, J.; Zhang, L.; Wang, J. Mineralogical Composition and Organic Matter Characteristics of Lacustrine Fine-Grained Volcanic-Hydrothermal Sedimentary Rocks: A Data-Driven Analytics for the Second Member of Permian Lucaogou Formation, Santanghu Basin, NW China. *Mar. Pet. Geol.* **2021**, *126*, 104920. [CrossRef]
28. Zhang, Q.; Wu, S.; Dong, D. Cenozoic Magmatism in the Northern Continental Margin of the South China Sea: Evidence from Seismic Profiles. *Mar. Geophys. Res.* **2016**, *37*, 71–94. [CrossRef]
29. Zhang, K.; Liu, R.; Liu, Z.; Li, B.; Han, J.; Zhao, K. Influence of Volcanic and Hydrothermal Activity on Organic Matter Enrichment in the Upper Triassic Yanchang Formation, Southern Ordos Basin, Central China. *Mar. Pet. Geol.* **2020**, *112*, 104059. [CrossRef]
30. Yang, X.; Yan, D.; Zhang, B.; Zhang, L.; Wei, X.; Li, T.; Zhang, J.; She, X. The Impact of Volcanic Activity on the Deposition of Organic-Rich Shales: Evidence from Carbon Isotope and Geochemical Compositions. *Mar. Pet. Geol.* **2021**, *128*, 105010. [CrossRef]
31. Rutman, P.; Hoareau, G.; Kluska, J.M.; Lejay, A.; Fialips, C.; Gelin, F.; Aubourg, C.; Bilbao, E.H. Diagenesis and Alteration of Subsurface Volcanic Ash Beds of the Vaca Muerta Formation, Argentina. *Mar. Pet. Geol.* **2021**, *132*, 105220. [CrossRef]
32. Liu, Q.; Li, P.; Jin, Z.; Liang, X.; Zhu, D.; Wu, X.; Meng, Q.; Liu, J.; Fu, Q.; Zhao, J. Preservation of Organic Matter in Shale Linked to Bacterial Sulfate Reduction (BSR) and Volcanic Activity under Marine and Lacustrine Depositional Environments. *Mar. Pet. Geol.* **2021**, *127*, 104950. [CrossRef]
33. Jiao, X.; Liu, Y.Q.; Yang, W.; Zhou, D.W.; Bai, B.; Zhang, T.S.; Zhao, M.R.; Li, Z.X.; Meng, Z.Y.; Yang, Y.Y.; et al. Fine-Grained Volcanic-Hydrothermal Sedimentary Rocks in Permian Lucaogou Formation, Santanghu Basin, NW China: Implications on Hydrocarbon Source Rocks and Accumulation in Lacustrine Rift Basins. *Mar. Pet. Geol.* **2020**, *114*, 104201. [CrossRef]
34. Cui, H.; Zhu, S.; Tan, M.; Tong, H. Depositional and Diagenetic Processes in Volcanic Matrix-Rich Sandstones from the Shanxi and Shihezi Formations, Ordos Basin, China: Implication for Volcano-Sedimentary Systems. *Basin Res.* **2022**, *34*, 1859–1893. [CrossRef]
35. Chen, H.; Zhu, X.; Gawthorpe, R.L.; Wood, L.J.; Liu, Q.; Li, S.; Shi, R.; Li, H. The Interactions of Volcanism and Clastic Sedimentation in Rift Basins: Insights from the Palaeogene-Neogene Shaleitian Uplift and Surrounding Sub-Basins, Bohai Bay Basin, China. *Basin Res.* **2021**, *34*, 1084–1112. [CrossRef]
36. Liu, Q.; Zhu, D.; Jin, Z.; Meng, Q.; Li, S. Influence of Volcanic Activities on Redox Chemistry Changes Linked to the Enhancement of the Ancient Sinian Source Rocks in the Yangtze Craton. *Precambrian Res.* **2019**, *327*, 1–13. [CrossRef]
37. Liu, G.; Zhai, G.; Huang, Z.; Zou, C.; Xia, X.; Shi, D.; Zhou, Z.; Zhang, C.; Chen, R.; Yu, S.; et al. The Effect of Tuffaceous Material on Characteristics of Different Lithofacies: A Case Study on Lucaogou Formation Fine-Grained Sedimentary Rocks in Santanghu Basin. *J. Pet. Sci. Eng.* **2019**, *179*, 355–377. [CrossRef]
38. Wang, K.; Xu, W.; Fu, M.; Deng, H.; Wang, X. Geochemical Transformation of Tuffaceous Materials in Tight Sandstone and Its Significance for Reservoir Reconstruction: A Case Study from the Taiyuan and Shihezi Formation in Dingbei Area, Ordos Basin. *Interpretation* **2022**, *10*, T739–T747. [CrossRef]
39. Zhou, N.; Lu, J.; Lu, S.; Zhang, P.; Wang, M.; Lin, Z.; Jiang, X.; Liu, Y.; Xiao, G. Depositional and Diagenetic Controls over Reservoir Quality of Tight Sandstone and Conglomerate in the Lower Cretaceous Shahezi Formation, Xujiaweizi Fault Depression, Songliao Basin, China. *Mar. Pet. Geol.* **2023**, *155*, 106374. [CrossRef]
40. Wang, Y.; Cheng, H.; Hu, Q.; Liu, L.; Hao, L. Diagenesis and Pore Evolution for Various Lithofacies of the Wufeng-Longmaxi Shale, Southern Sichuan Basin, China. *Mar. Pet. Geol.* **2021**, *133*, 105251. [CrossRef]
41. Worden, R.H.; Bukar, M.; Shell, P. The Effect of Oil Emplacement on Quartz Cementation in a Deeply Buried Sandstone Reservoir. *Am. Assoc. Pet. Geol. Bull.* **2018**, *102*, 49–75. [CrossRef]
42. Alessandretti, L.; Philipp, R.P.; Chemale, F.; Brückmann, M.P.; Zvirtes, G.; Matté, V.; Ramos, V.A. Provenance, Volcanic Record, and Tectonic Setting of the Paleozoic Ventania Fold Belt and the Claromecó Foreland Basin: Implications Onsedimentation and Volcanism along the Southwestern Gondwana Margin. *J. S. Am. Earth Sci.* **2013**, *47*, 12–31. [CrossRef]
43. Arif, M.; Dey, S.; Gond, A.K.; Zong, K.; Liu, Y.; Mitra, A.; Mitra, A.; Sarangi, S. Mesoarchean Continental Intraplate Volcanism and Sedimentation: The Case of the Simlipal Basin, Singhbhum Craton, Eastern India. *Precambrian Res.* **2021**, *361*, 106245. [CrossRef]
44. Rossignol, C.; Hallot, E.; Bourquin, S.; Poujol, M.; Jolivet, M.; Pellenard, P.; Ducassou, C.; Nalpas, T.; Heilbronn, G.; Yu, J.; et al. Using Volcaniclastic Rocks to Constrain Sedimentation Ages: To What Extent Are Volcanism and Sedimentation Synchronous? *Sediment. Geol.* **2019**, *381*, 46–64. [CrossRef]
45. Manikyamba, C.; Saha, A.; Ganguly, S.; Santosh, M.; Lingadevaru, M.; Rajanikanta Singh, M.; Subba Rao, D.V. Sediment-Infill Volcanic Breccia from the Neoarchean Shimoga Greenstone Terrane, Western Dharwar Craton: Implications on Pyroclastic Volcanism and Sedimentation in an Active Continental Margin. *J. Asian Earth Sci.* **2014**, *96*, 269–278. [CrossRef]
46. Pelullo, C.; Arienzo, I.; D'Antonio, M.; Giaccio, B.; Iovine, R.S.; Leicher, N.; Palladino, D.M.; Petrelli, M.; Petrosino, P.; Russo Ermolli, E.; et al. Explosive Volcanic Activity in Central-Southern Italy during Middle Pleistocene: A Tale from Tephra Layers of the Acerno Basin. *Quat. Sci. Adv.* **2024**, *14*, 100186. [CrossRef]
47. Meng, Z.; Liu, Y.; Jiao, X.; Ma, L.; Zhou, D.; Li, H.; Cao, Q.; Zhao, M.; Yang, Y. Petrological and Organic Geochemical Characteristics of the Permian Lucaogou Formation in the Jimsar Sag, Junggar Basin, NW China: Implications on the Relationship between Hydrocarbon Accumulation and Volcanic-Hydrothermal Activities. *J. Pet. Sci. Eng.* **2022**, *210*, 110078. [CrossRef]

48. Cao, Y.; Kang, Z.; Yang, F.; Zhou, T.; Liu, D.; Wang, R. Geochronology, Geochemistry and Geological Significance of Volcanic Rocks of the Bangba District, Western Segment of the Central Lhasa Subterrane. *J. Earth Sci.* **2022**, *33*, 681–695. [CrossRef]
49. Lu, Z.; He, Z.; Gluyas, J.G.; Liu, G.; Liu, T.; Chen, C.; Zou, M. Reservoir Quality of the Lower–Middle Permian Shan 2 and He 1 Members in the Ordos Basin, China: Implications for Depositional and Diagenetic Processes and the Role of Volcanic Tuffaceous Sediment in Tight Sandstones. *J. Asian Earth Sci.* **2024**, *263*, 106050. [CrossRef]
50. Escuder-Viruete, J.; Molina, E.A.; Chinchilla, D.; Gabites, J.; Seggiaro, R.; Marquetti, C.A.; Heredia, N. Structural and Temporal Relationships between Volcanic Activity, Hydrothermal Alteration, Epithermal Ag–Pb–Zn Mineralization and Regional Stress Regime in the Quevar Volcanic Complex (Puna Plateau, Salta Province, NW Argentina). *J. Struct. Geol.* **2022**, *158*, 104582. [CrossRef]
51. Qin, P.; Han, D.; Ma, B.; Zeng, X.; Lin, Y. Diagenetic Differentiation of Tuffaceous Interstitial Materials in Sandy Conglomerate and Their Effect on Reservoir Properties. *Mar. Pet. Geol.* **2023**, *157*, 106476. [CrossRef]
52. Imura, T.; Ban, M.; Tsunematsu, K.; Goto, A.; Okada, J.; Kuri, M. Geological Constraints on Volcanic-Fluid Pathways at the Maruyamasawa-Fumarolic-Geothermal-Area, and Its Relation to the Present Magmatic-Hydrothermal Activity in Zao Volcano, Tohoku, Japan. *J. Volcanol. Geotherm. Res.* **2023**, *437*, 107793. [CrossRef]
53. Suárez, M.; De La Cruz, R.; Aguirre-Urreta, B.; Fanning, M. Relationship between Volcanism and Marine Sedimentation in Northern Austral (Aisén) Basin, Central Patagonia: Stratigraphic, U-Pb SHRIMP and Paleontologic Evidence. *J. S. Am. Earth Sci.* **2009**, *27*, 309–325. [CrossRef]
54. Martínez-Paco, M.; Velasco-Tapia, F.; Santana-Salas, L.A.; Juárez-Arriaga, E.; Aceves de Alba, J.; Ernesto Ocampo-Díaz, Y.Z. San Felipe and Caracol Tuffaceous Sandstones, NE Mexico—Late Cretaceous Continental Arc Petrogenetic Link: Petrographic, Geochemical, and Geochronological Evidence. *J. S. Am. Earth Sci.* **2022**, *116*, 103818. [CrossRef]
55. Marsaglia, K.M.; Barone, M.; Critelli, S.; Busby, C.; Fackler-Adams, B. Petrography of Volcaniclastic Rocks in Intra-Arc Volcano-Bounded to Fault-Bounded Basins of the Rosario Segment of the Lower Cretaceous Alisitos Oceanic Arc, Baja California, Mexico. *Sediment. Geol.* **2016**, *336*, 138–146. [CrossRef]
56. Fisher, R.V.; Smith, G.A. *Sedimentation in Volcanic Settings*; SEPM Society for Sedimentary Geology: Tulsa, Oklahoma, 1991.
57. Brandl, P.A.; Hamada, M.; Arculus, R.J.; Johnson, K.; Marsaglia, K.M.; Savov, I.P.; Ishizuka, O.; Li, H. The Arc Arises: The Links between Volcanic Output, Arc Evolution and Melt Composition. *Earth Planet. Sci. Lett.* **2017**, *461*, 73–84. [CrossRef]
58. Cas, R.A.F.; Wright, J.V. *Volcanic Successions Modern and Ancient: A Geological Approach to Processes, Products and Successions*, 1st ed.; Cas, R.A.F., Wright, J.V., Eds.; Springer: Dordrecht, The Netherlands, 1988; ISBN 978-94-009-3167-1.
59. Di Capua, A.; De Rosa, R.; Kereszturi, G.; Le Pera, E.; Rosi, M.; Watt, S.F.L. Volcanically-Derived Deposits and Sequences: A Unified Terminological Scheme for Application in Modern and Ancient Environments. In *Volcanic Processes in the Sedimentary Record: When Volcanoes Meet the Environment*; Di Capua, A., De Rosa, R., Kereszturi, G., Le Pera, E., Rosi, M., Watt, S.F.L., Eds.; Geological Society of London: London, UK, 2023; pp. 11–27. ISBN 9781786205667.
60. Di Capua, A.; De Rosa, R.; Kereszturi, G.; Le Pera, E.; Rosi, M.; Watt, S.F.L. From Volcanoes to Sedimentary Systems. In *Volcanic Processes in the Sedimentary Record: When Volcanoes Meet the Environment*; Di Capua, A., De Rosa, R., Kereszturi, G., Le Pera, E., Rosi, M., Watt, S.F.L., Eds.; Geological Society of London: London, UK, 2023; pp. 1–9. ISBN 9781786205667.
61. Chang, J. Forced-Regressive Sand Bodies and the Related Lithologic Reservoirs of Zhujiang Formation in Huizhou Sag, Pearl River Mouth Basin. *Mar. Orig. Pet. Geol.* **2020**, *25*, 121–131.
62. Duan, W.; Shi, L.; Luo, C.; Li, S. Hydrocarbon Accumulation Mechanism in the Far-Source Reservoirs of Dongsha Uplift of the Pearl River Mouth Basin, Northern South China Sea. *J. Pet. Sci. Eng.* **2022**, *220*, 111145. [CrossRef]
63. Lin, H.M.; Liu, H.; Wang, X.D.; Qiu, X.W.; Ju, Y.T.; Meng, J.; Li, L. Basin-Filling Processes and Hydrocarbon Source Rock Prediction of Low-Exploration Degree Areas in Rift Lacustrine Basins: A Case from the Wenchang Formation in Low-Exploration Degree Areas, Northern Zhu I Depression, Pearl River Mouth Basin, E China. *J. Palaeogeogr.* **2022**, *11*, 286–313. [CrossRef]
64. Liu, E.; Chen, S.; Yan, D.; Deng, Y.; Wang, H.; Jing, Z.; Pan, S. Detrital Zircon Geochronology and Heavy Mineral Composition Constraints on Provenance Evolution in the Western Pearl River Mouth Basin, Northern South China Sea: A Source to Sink Approach. *Mar. Pet. Geol.* **2022**, *145*, 105884. [CrossRef]
65. Wang, W.; Zeng, Z.; Yang, X.; Bidgoli, T. Exploring the Roles of Sediment Provenance and Igneous Activity on the Development of Synrift Lacustrine Source Rocks, Pearl River Mouth Basin, Northern South China Sea. *Mar. Pet. Geol.* **2022**, *147*, 105990. [CrossRef]
66. Chen, W.; Du, J.; Shi, H.; He, M. Compound Hydrocarbon Accumulation and Enrichment in Southwestern Huizhou Sag, Pearl River Mouth Basin, South China Sea. *Pet. Explor. Dev.* **2015**, *42*, 215–222. [CrossRef]
67. Ge, J.; Zhao, X.; Zhu, X.; Liao, J.; Ma, B.; Jones, B.G. Tectono-Sedimentary Signature of the Second Rift Phase in Multiphase Rifts: A Case Study in the Lufeng Depression (38–33.9 Ma), Pearl River Mouth Basin, South China Sea. *Mar. Pet. Geol.* **2020**, *114*, 104218. [CrossRef]
68. Zhao, Q.; Zhu, H.; Zhang, X.; Liu, Q.; Qiu, X.; Li, M. Geomorphologic Reconstruction of an Uplift in a Continental Basin with a Source-to-Sink Balance: An Example from the Huizhou-Lufeng Uplift, Pearl River Mouth Basin, South China Sea. *Mar. Pet. Geol.* **2021**, *128*, 104984. [CrossRef]
69. Hui, G.; Zhang, P.; Li, Z.; Wang, W.; Hu, L.; Li, G.; Zhang, Y.; Sun, C.; Li, S.; Liang, H.; et al. Opening of the South China Sea Marginal Basin: Insights from the Tectonic Evolution of the ENE-Striking Littoral Fault Zone. *Mar. Pet. Geol.* **2022**, *145*, 105854. [CrossRef]

70. Mu, D.; Peng, G.; Zhu, D.; Li, S.; Suo, Y.; Zhan, H.; Zhao, L. Structure and Formation Mechanism of the Pearl River Mouth Basin: Insights from Multi-Phase Strike-Slip Motions in the Yangjiang Sag, SE China. *J. Asian Earth Sci.* **2022**, *226*, 105081. [CrossRef]
71. Zeng, Z.; Zhu, H.; Yang, X.; Zeng, H.; Xia, C.; Chen, Y. Using Seismic Geomorphology and Detrital Zircon Geochronology to Constrain Provenance Evolution and Its Response of Paleogene Enping Formation in the Baiyun Sag, Pearl River Mouth Basin, South China Sea: Implications for Paleo-Pearl River Drainage Evoluti. *J. Pet. Sci. Eng.* **2019**, *177*, 663–680. [CrossRef]
72. Peng, J.; Pang, X.; Peng, H.; Ma, X.; Shi, H.; Zhao, Z.; Xiao, S.; Zhu, J. Geochemistry, Origin, and Accumulation of Petroleum in the Eocene Wenchang Formation Reservoirs in Pearl River Mouth Basin, South China Sea: A Case Study of HZ25-7 Oil Field. *Mar. Pet. Geol.* **2017**, *80*, 154–170. [CrossRef]
73. Shi, H.; Du, J.; Mei, L.; Zhang, X.; Hao, S.; Liu, P.; Deng, P.; Zhang, Q. Huizhou Movement and Its Significance in Pearl River Mouth Basin, China. *Pet. Explor. Dev.* **2020**, *47*, 483–498. [CrossRef]
74. Wang, X.; He, S.; Wu, J. Tectonic Controls on Lacustrine Source Rock Occurrence in the Huizhou Sag, Pearl River Mouth Basin, China. *Int. Geol. Rev.* **2020**, *62*, 72–93. [CrossRef]
75. Dickson, J.A.D. Carbonate Identification and Genesis as Revealed by Staining. *J. Sediment. Res.* **1966**, *36*, 491–505. [CrossRef]
76. Dickson, J.A.D. A Modified Staining Technique for Carbonates in Thin Section. *Nature* **1965**, *205*, 4971. [CrossRef]
77. Zuffa, G.G. Optical Analyses of Arenites: Influence of Methodology on Compositional Results BT—Provenance of Arenites. In *Provenance of Arenites*; Zuffa, G.G., Ed.; Springer: Dordrecht, The Netherlands, 1985; pp. 165–189. ISBN 978-94-017-2809-6.
78. Ingersoll, R.V.; Bullard, T.F.; Ford, R.L.; Grimm, J.P.; Pickle, J.D.; Sares, S.W. The Effect of Grain Size on Detrital Modes: A Test of the Gazzi-Dickinson Point-Counting Method. *J. Sediment. Res.* **1984**, *54*, 103–116. [CrossRef]
79. Dickinson, W.R. Interpreting Detrital Modes of Graywacke and Arkose. *J. Sediment. Res.* **1970**, *40*, 695–707. [CrossRef]
80. *SY-T 6385-1999*; The Porosity and Permeability Measurement of Core in the Net Confining Stress. State Bureau of Petroleum and Chemical Industries: Beijing, China, 1999.
81. Ma, B.; Gao, J.; Eriksson, K.A.; Zhu, H.; Liu, Q.; Ping, X.; Zhang, Y. Diagenetic Alterations in Eocene, Deeply Buried Volcaniclastic Sandstones with Implications for Reservoir Quality in the Huizhou Depression, Pearl River Mouth. *Am. Assoc. Pet. Geol. Bull.* **2023**, *107*, 929–955. [CrossRef]
82. Chen, S.; Xian, B.; Ji, Y.; Ll, J.; Tian, R.; Wang, P.; Tang, H. Influences of Burial Process on Diagenesis and High-Quality Reservoir Development of Deep–Ultra-Deep Clastic Rocks: A Case Study of Lower Cretaceous Qingshuihe Formation in Southern Margin of Junggar Basin, NW China. *Pet. Explor. Dev.* **2024**, *51*, 364–379. [CrossRef]
83. Garzanti, E.; Andò, S.; Limonta, M.; Fielding, L.; Najman, Y. Diagenetic Control on Mineralogical Suites in Sand, Silt, and Mud (Cenozoic Nile Delta): Implications for Provenance Reconstructions. *Earth Sci. Rev.* **2018**, *185*, 122–139. [CrossRef]
84. Folk, R.L. *Petrology of Sedimentary Rocks*; Hemphill Publishing Company: Austin, TX, USA, 1974.
85. Yuan, G.; Peng, G.; Zhang, L.; Sun, H.; Chen, S.; Liu, H.; Zhao, X. Diagenesis and Low-Permeability Tightening Mechanisms of the Deep Paleogene Reservoirs under High Temperature and Highly Variable Geothermal Gradients in the Baiyun Sag, Pearl River Mouth Basin. *Oil Gas Geol.* **2024**, *45*, 44–64.
86. Liu, D.; Sun, W.; Ren, D.; Li, C. Quartz Cement Origins and Impact on Storage Performance in Permian Upper Shihezi Formation Tight Sandstone Reservoirs in the Northern Ordos Basin, China. *J. Pet. Sci. Eng.* **2019**, *178*, 485–496. [CrossRef]
87. Oye, O.J.; Aplin, A.C.; Jones, S.J.; Gluyas, J.G.; Bowen, L.; Harwood, J.; Orland, I.J.; Valley, J.W. Vertical Effective Stress and Temperature as Controls of Quartz Cementation in Sandstones: Evidence from North Sea Fulmar and Gulf of Mexico Wilcox Sandstones. *Mar. Pet. Geol.* **2020**, *115*, 104289. [CrossRef]
88. Yu, Y.; Lin, L.; Li, Z.; Chen, H. Source of Quartz Cement in Tight Gas Sandstone: Evidence from the Upper Triassic Xujiahe Formation in the Western Sichuan Basin, SW China. *J. Pet. Sci. Eng.* **2022**, *212*, 110299. [CrossRef]
89. Chen, S.; Yang, Y.; Qiu, L.; Wang, X.; Habilaxim, E. Source of Quartz Cement and Its Impact on Reservoir Quality in Jurassic Shaximiao Formation in Central Sichuan Basin, China. *Mar. Pet. Geol.* **2024**, *159*, 106543. [CrossRef]
90. Schmidt, V.; Mcdonald, D.A. The Role of Secondary Porosity in the Course of Sandstone Diagenesis. *Asp. Diagenes.* **1979**, *26*, 175–207.
91. Yang, P.; Zhang, L.; Liu, K.; Cao, B.; Gao, J.; Qiu, G. Diagenetic History and Reservoir Evolution of Tight Sandstones in the Second Member of the Upper Triassic Xujiahe Formation, Western Sichuan Basin, China. *J. Pet. Sci. Eng.* **2021**, *201*, 108451. [CrossRef]
92. Ma, J.; Liu, G.; Huang, Z.; Ou, G.; Li, T.; Guo, X. Tight Tuff Reservoir Characteristics and Its Controlling Factors: A Comparative Study of the Permian Tiaohu Formation and Carboniferous Haerjiawu Formation in the Santanghu Basin, NW China. *J. Pet. Sci. Eng.* **2020**, *187*, 106808. [CrossRef]
93. Ma, J.; Huang, Z.; Zhong, D.; Liang, S.; Liang, H.; Xue, D.; Chen, X.; Fan, T. Formation and Distribution of Tuffaceous Tight Reservoirs in the Permian Tiaohu Formation in the Malang Sag, Santanghu Basin, NW China. *Pet. Explor. Dev.* **2016**, *43*, 778–786. [CrossRef]
94. Xiang, F.; Yu, X.; Huang, H.; Zhang, D.; Zhu, X. Mineralogical Characterization and Diagenetic History of Permian Marine Tuffaceous Deposits in Guangyuan Area, Northern Sichuan Basin, China. *Mar. Pet. Geol.* **2021**, *123*, 104744. [CrossRef]
95. Cheng, R.; Shen, Y.; Yan, J.; Li, Q.; Li, X.; Wang, Y.; Li, F.; Xu, Z. Diagenesis of Volcaniclastic Rocks in Hailaer Basin. *Acta Petrol. Sin.* **2010**, *26*, 47–54.
96. Le Maitre, R.W. *Igneous Rocks: A Classification and Glossary of Terms: Recommendations of the International Union of Geological Sciences Subcommission on the Systematics of Igneous Rocks*, 2nd ed.; Cambridge University Press: Cambridge, UK, 2005; ISBN 9780521619486.

97. Paxton, S.T.; Szabo, J.O.; Ajdukiewicz, J.M.; Klimentidis, R.E. Construction of an Intergranular Volume Compaction Curve for Evaluating and Predicting Compaction and Porosity Loss in Rigid-Grain Sandstone Reservoirs. *Am. Assoc. Pet. Geol. Bull.* **2002**, *86*, 2047–2067. [CrossRef]
98. Liu, K.; Wang, R.; Shi, W.; Travé, A.; Martín-Martín, J.D.; Baqués, V.; Qi, R.; Lin, J.; Ye, H. Diagenetic Controls on Reservoir Quality and Heterogeneity of the Triassic Chang 8 Tight Sandstones in the Binchang Area (Ordos Basin, China). *Mar. Pet. Geol.* **2022**, *146*, 105974. [CrossRef]
99. Xu, W.; Wen, H.; Lu, Z.; Zhong, K.; Feng, Q.; Luo, B.; Liao, Y.; Zhou, G. Diagenetic Evolution and Its Impact on Reservoir Porosity in Lower Triassic Jialingjiang Formation in Eastern Sichuan Basin, SW China: Evidence from Petrography, Trace Elements, and Isotopic Studies. *J. Pet. Sci. Eng.* **2022**, *208*, 109341. [CrossRef]
100. Cao, Z.; Azmy, K.; Lin, C.; Dong, C.; Ren, L.; Qin, M.; Li, Z.; Tan, X.; Zhang, L.; Li, X. Diagenetic Evolution of the Lower Yaojia Formation of Songliao Basin, China: Impact on Reservoir Quality. *J. Pet. Sci. Eng.* **2022**, *213*, 110415. [CrossRef]
101. Zhao, X.; Yao, G.; Chen, X.; Zhang, R.; Lan, Z.; Wang, G. Diagenetic Facies Classification and Characterization of a High-Temperature and High-Pressure Tight Gas Sandstone Reservoir: A Case Study in the Ledong Area, Yinggehai Basin. *Mar. Pet. Geol.* **2022**, *140*, 105665. [CrossRef]
102. Ehrenberg, S.N.; Nadeau, P.H.; Steen, Ø. Petroleum Reservoir Porosity versus Depth: Influence of Geological Age. *Am. Assoc. Pet. Geol. Bull.* **2009**, *93*, 1281–1296. [CrossRef]
103. Ehrenberg, S.N.; Nadeau, P.H. Sandstone vs. Carbonate Petroleum Reservoirs: A Global Perspective on Porosity-Depth and Porosity-Permeability Relationships. *Am. Assoc. Pet. Geol. Bull.* **2005**, *89*, 435–445. [CrossRef]
104. Khan, S.H.; Sheng, Y.M.; Critelli, S.; Civitelli, M.; Mughal, M.S.; Basharat, U. Depositional and Diagenetic Controls on Reservoir Properties of the Lower Cambrian Khewra Sandstone, Eastern Salt Range, Sub-Himalaya, Pakistan. *Mar. Pet. Geol.* **2024**, *161*, 106651. [CrossRef]
105. Marsaglia, K.M.; Carozzi, A.V. Depositional Environment, Sand Provenance, and Diagenesis of the Basal Salina Formation (Lower Eocene), Northwestern Peru. *J. S. Am. Earth Sci.* **1990**, *3*, 253–267. [CrossRef]
106. Cavazza, W.; Dahl, J. Note on the Temporal Relationships between Sandstone Compaction and Precipitation of Authigenic Minerals. *Sediment. Geol.* **1990**, *69*, 37–44. [CrossRef]
107. Wang, J.; Cao, Y.; Liu, K.; Liu, J.; Xue, X.; Xu, Q. Pore Fluid Evolution, Distribution and Water-Rock Interactions of Carbonate Cements in Red-Bed Sandstone Reservoirs in the Dongying Depression, China. *Mar. Pet. Geol.* **2016**, *72*, 279–294. [CrossRef]
108. Ma, W.; Cao, Y.; Xi, K.; Liu, K.; Lin, M.; Liu, J. Interactions between Mineral Evolution and Organic Acids Dissolved in Bitumen in Hybrid Shale System. *Int. J. Coal Geol.* **2022**, *260*, 104071. [CrossRef]
109. Marghani, M.M.A.; Zairi, M.; Radwan, A.E. Facies Analysis, Diagenesis, and Petrophysical Controls on the Reservoir Quality of the Low Porosity Fluvial Sandstone of the Nubian Formation, East Sirt Basin, Libya: Insights into the Role of Fractures in Fluid Migration, Fluid Flow, and Enhancing the P. *Mar. Pet. Geol.* **2023**, *147*, 105986. [CrossRef]
110. Fang, X.; Ma, C.; Zhao, L.; Lei, L.; Huang, W.; Han, C.; Qi, M. Diagenetic Evolution of Tight Sandstone and the Formation of an Effective Reservoir in the Lower Member 3 of the Shahejie Formation, Bohai Bay Basin, East China. *Mar. Pet. Geol.* **2024**, *161*, 106658. [CrossRef]
111. Yu, Z.; Cheng, R.; Zhao, X.; Sun, F. Types and Succession of Pyroclastic Rocks Diagenesis in Lower Cretaceous of Wuerxun and Bei'er Depression in Hailaer Basin. *Earth Sci.* **2012**, *37*, 851–859.
112. Zhou, J.; Liu, B.; Shao, M.; Yin, C.; Jiang, Y.; Song, Y. Lithologic Classification of Pyroclastic Rocks: A Case Study for the Third Member of the Huoshiling Formation, Dehui Fault Depression, Songliao Basin, NE China. *J. Pet. Sci. Eng.* **2022**, *214*, 110456. [CrossRef]
113. Mao, Z.; Fang, X.; Yang, Y.; Ye, C.; Zhang, W.; Zhang, T.; Christidis, G.E. Identification and Origin of the Late Oligocene to Miocene Pyroclastic Rocks in the Lunpola Basin and Link with Deep Geodynamics in the Lhasa Terrane, Tibetan Plateau. *J. Asian Earth Sci.* **2023**, *247*, 105575. [CrossRef]